Air-Transfer Production Method for Large-Area Picosecond Photodetectors

E. Angelico,[1] A. Elagin,[1] H. J. Frisch,[1] E. Spieglan,[1] B. W. Adams,[2, a)] M. R. Foley,[2] and M. J. Minot[2]
[1)]*Enrico Fermi Institute, University of Chicago, Chicago, IL 60637, USA*
[2)]*Incom Inc., Charlton, MA 01507, USA*

(Dated: 28 April 2020)

We have designed and prototyped the process steps for the batch production of large-area micro-channel-plate photomultipliers (MCP-PMT) using the "air-transfer" assembly process developed with single *LAPPD*^{TM} modules. Results are presented addressing the challenges of designing a robust package that can transmit large numbers of electrical signals for pad or strip readout from inside the vacuum tube, and of hermetically sealing the large-perimeter window-body interface. We have also synthesized a photocathode in a large-area low-aspect-ratio volume, and have shown that the micro-channel plates recover their functionality after cathode synthesis. These steps inform a design for a multi-module batch facility employing dual nested low-vacuum (LV) and ultra-high-vacuum (UHV) systems in a small-footprint. The facility design provides full access to multiple MCP-PMT modules prior to hermetic pinch-off for leak-checking and real-time photocathode optimization.

I. INTRODUCTION

Applications for large-area coverage of photodetectors with excellent time and space resolution include: a) correlated precision time and space information in high-energy particle collider and fixed-target events[1]; b) simultaneous measurements in near and far detectors of neutrino oscillations using time-selected energy spectra[2]; c) imaging double-beta decay events in large liquid scintillator detectors using timing to separate Cherenkov and scintillation light[3–8]; d) reconstruction of neutral mesons decaying to photons in searches for rare meson decays[9–11]; e) low-dose whole body Time-of-Flight Positron-Emission Tomography[12–15]; and e) nuclear non-proliferation and reactor monitoring[16].

The typical method of production of commercial photomultipliers (PMT) is in a batch production station that processes multiple modules per cycle. Figure 1 shows a commercial PMT station[17] purchased by the LAPPD Collaboration[18]. The PMT process steps served as the model for the development of the batch production process for large-area flat-panel micro-channel-plate-based (MCP-based) photodetectors (MCP-PMT) [19,20].

The salient features that form the basis of the design for flat-panel photodetector production are as follows[17]. During processing the PMT glass envelopes are at ultra-high vacuum (UHV) internally and are at atmosphere externally. The initial evacuation of the phototube is at low vacuum (LV), performed by an external pump through long low-conductance plumbing, with the PMT glass envelopes connected through a narrow tubulation sealed by a low-vacuum O-ring gland. An oven is placed over the assembly for bake-out and subsequent photocathode formation. The antimony pre-cursor layer is evaporated by line-of-sight onto the inside surface of the entrance window, and the alkali vapor is generated by sources inside the glass envelope. The UHV inside the tube is provided by the bake-out, the internal getter, and the alkali vapors, and not by the external pump. After cathode optimization the tubulation is pinched off hermetically sealing the phototube with the getter inside.

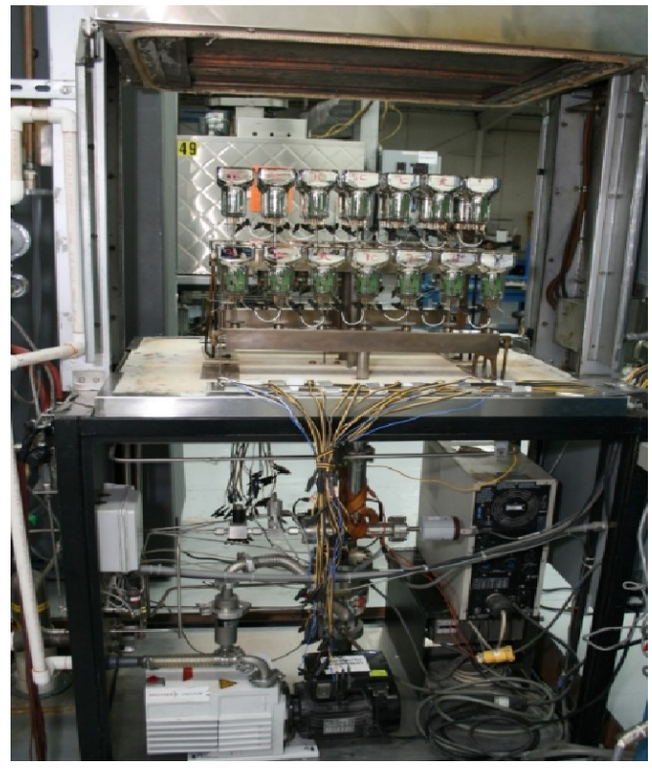

FIG. 1. The photomultiplier batch production station purchased from the Photonis Lancaster plant[17] that served as the model for development of the LAPPD batch production process.

Experience with the process steps used for the Photonis PMT station guided the development of the process for large-area micro-channel-plate-based PMT batch production described below. However, large-area MCP-PMTs present unique challenges, requiring: 1) a robust package that can

a)Current Address: Quantum Optics Applied Research, Naperville, IL 60565, USA

transmit large numbers of electrical signals for pad or strip readout from inside the vacuum volume; 2) hermetically sealing the large-circumference window-body interface; 3) synthesizing the photocathode in a large flat package; and 4) recovery of the functionality of the large surface-area MCPs after cathode synthesis.

The synthesis of bialkali photocathodes by exposing an antimony (Sb) layer pre-deposited on a substrate by thermal evaporation was described by Sinclair in 2009[21]. This suggestion led to a DOE-funded development program for a theory-based K_2CsSb cathode in a collaboration of the University of Chicago (UC), Brookhaven National Laboratory (BNL) and Radiation Monitoring Devices (RMD, Inc.)[22–25]. However, we recently discovered that the chemistry of photocathode synthesis based on a pre-deposited Sb layer had been explored in detail by Barois et al. in 1989[26,27], and that the air-transfer process is currently being used commercially in Russia to make multi-anode photomultipliers[28]. Hamamatsu also processes some of their phototubes using the air-transfer process[29].

The Barois insitu photocathode process tightly controls the uniformity of the cathode layer through the thickness of the Sb precursor layer, which can be made highly uniform by conventional thermal evaporation[30]. The chemical and physical composition of the structure is determined by a number of parameters as discussed in Refs[22–25], and has the attractive property that the reaction runs to completion.

Specific Cs-Sb compounds may be formed by equilibrium reaction of Sb with Cs vapor[27], the stoichiometry set by temperatures and pressures in the system. Some stoichiometries are optimal for high quantum efficiency. Since the Sb is immobile, a cathode of uniform thickness and composition can be produced from an Sb layer of uniform thickness and crystal structure[24,25,30].

II. THE DUAL-VACUUM AIR-TRANSFER METHOD

The LV/UHV-dual-vacuum technique uses an outer vacuum vessel which contains the photodetector module. The outer vessel provides thermal insulation for a high-temperature bakeout of the photodetector module ("tile"), reduces the formation of oxides in the solder during heating, and ensures that no mechanical pressure differential exists across the molten seal. The module is assembled with the entrance window clamped in place, and is connected through a tubulation or tubulations to an independent UHV manifold and pump. Initially, before the hermetic seal is formed during the bake-out thermal cycle, the two vacuum systems can communicate through the unsealed seam between the window and the tile base. The bake-out cycle forms the seal between the window and base, and activates the getter in the module. After cooling below the seal melting temperature the two vacuum systems are independent, and the outer vacuum can be opened to atmosphere. The inner vacuum system is used as a source for the alkali vapors to synthesize the photocathode from the Sb precursor layer on the window.

Figure 2 shows the outer vacuum vessel. The vacuum pump for the outer system is on the left; the connections to the inner vacuum system enter through the flange on the bottom. The upper part of the vessel can be lifted off after sealing, exposing the sealed module for leak-checking and subsequent photocathode synthesis.

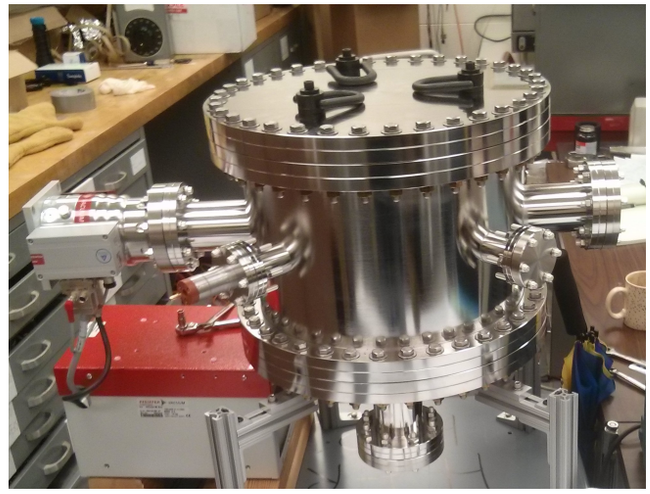

FIG. 2. The outer LV vacuum vessel that provides thermal insulation to the photodetector module during bake-out, a low oxidation environment, and equalization of the pressure across the molten indium alloy seal.

The inner UHV vacuum system consists of the tile volume, copper tubulations, and the manifold that connects the tile to the inner system vacuum pump and the alkali vapor source. A diagram of the manifold and the associated component process temperatures during alkali transport is shown in Figure 3.

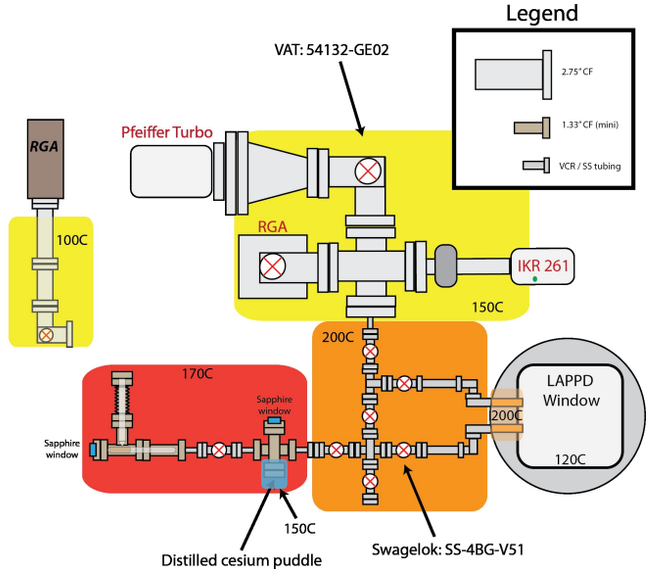

FIG. 3. The physical layout and associated component process temperatures during alkali vapor transport of the UHV inner vacuum manifold.

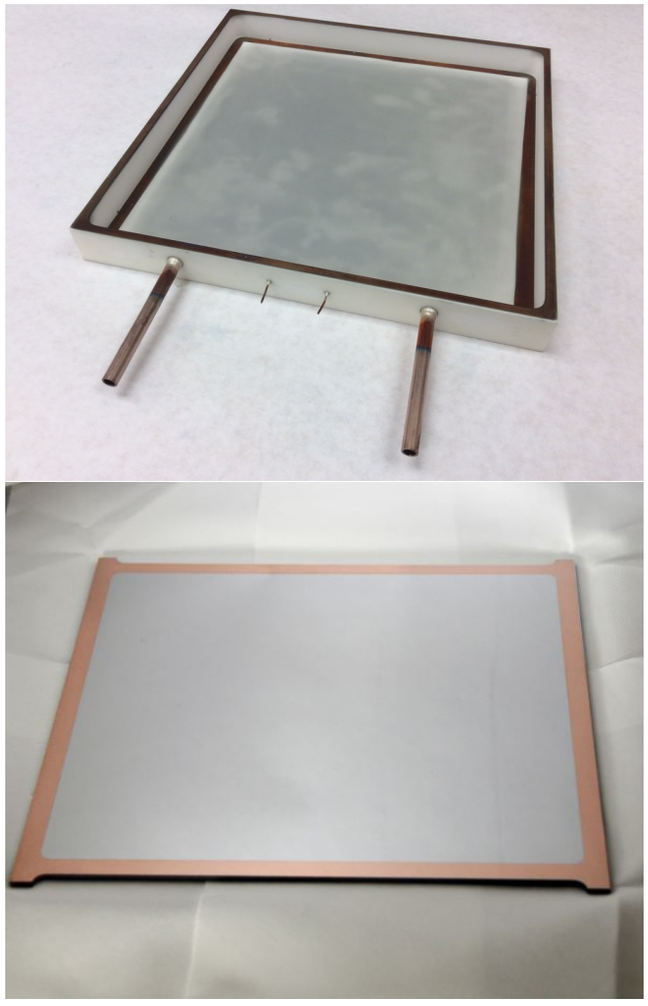

FIG. 4. Top: A two-pin ceramic tile body with metalized sealing surface and NiCr capacitively-coupled anode; Bottom: An entrance window with metalized sealing surface.

III. THE LAPPD^{TM} PACKAGE

The UC ceramic tile package consists of a monolithic ceramic tile base with capacitively coupled anode and a transparent entrance window, shown in Figure 4. The fast signal pulses are capacitively coupled through the anode on the bottom plate[31], avoiding the difficulty in brazing a large number of pins.

The tile base is one-piece, composed of high-purity Al_2O_3 ceramic[32,33]. Two 1/4" OFHC copper tubes are brazed through the sidewall to provide for pump-down and alkali vapor transport. Current designs incorporate 6 copper pins, 3 per side, brazed through opposing sidewalls for HV distribution to the cathode, amplification section, and anode[33]. Figure 5 shows a ceramic sidewall with pins and tubes.

The top surface of the tile base sidewall is the surface that mates with the window to provide the hermetic seal. The solder seal requires that this surface be metalized. The majority of the trials used thin film evaporation to deposit 200 nm

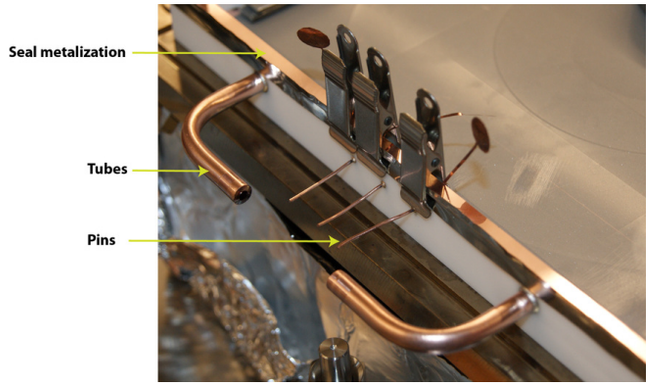

FIG. 5. Copper tubes that connect the tile base to the UHV manifold, and copper pins that provide HV to the cathode and amplification stack.

of 80-20 NiCr followed by 200 nm of Cu without a vacuum break[33] on the sealing surface, with the sidewall and anode tile surfaces protected by masks.

The bottom interior surface of the tile was also coated by evaporation. The first step was evaporation of 10 nm of NiCr on the active area of the anode to provide capacitive coupling to the external signal board[31]. A second set of masks was used to deposit 200 nm of NiCr followed by 200 nm of Cu, also without a vacuum break, for a narrow border overlapping the 10 nm NiCr anode to provide electrical contact[33].

The UHV inside the module is maintained after sealing by an internal non-evaporative getter consisting of two stacks each containing six 174-mm by 8-mm strips of SAES ST707[34] held in clips soldered to the anode.

The mating surface of the window was also metalized by evaporation[33] using successive masks[35]. First 200 nm of NiCr was deposited on the border with thin 'fingers' toward the center to distribute current across the cathode. A second evaporation deposited 200 nm of Cu on the Ni border for the indium alloy solder bond. A third evaporation deposited a thin Sb film as the pre-cursor for the alkali cathode.

The unsupported spans of the window and tile base anode surface need to support almost 1000 lbs of compressive atmospheric pressure. Sixteen columns of 3/8"-diameter ceramic cylinders ("buttons") are placed internally at 1.8" spacing in the gaps between the window, MCP's, and anode. The buttons serve three purposes:

1. Supporting the package against the compressive force of atmospheric pressure on the top and bottom of the package;
2. Setting the gaps between the MCP's, tile base, and the photocathode;
3. Applying mechanical force between the MCP surfaces and the high-voltage internal electrodes that connect the accelerating high voltages to their respective pins through the sidewall.

The left-hand panel of Figure 6 shows the placement of the button columns and the internal high-voltage electrodes connected to the side-wall pins during the first stage of assembly.

Atmospheric pressure is used to constrain the amplification stack against lateral motion; the right-hand panel shows the predicted stress for a 2.75 mm-thick B33 glass window.

The amplification section consists of two ALD-coated 20 cm-square MCPs in a chevron configuration[36–38]. The spacing between plates is set by button spacers to 0.080"; the spacing between the top or bottom plate and the top (cathode) or bottom (anode) surfaces, respectively, is similarly set to 0.25". The capillary seal (see Section IV) reduces the necessary assembly tolerances by precisely determining the indium layer thickness via a 'hard-stop' in the seal gap rather than by the stack height. The measured precision on the column heights is 0.5 mils. Before assembling the tile the micro-channel plates were vacuum-baked and scrubbed with a UV lamp.

The monolithic ceramic tile avoids the problem of having many penetrations to bring the signals out by capacitively coupling through the thin metal anode to an external signal pickup board[31]. The signal board is customized to use microstrips[39,40] or pads[31], determined by the application.

IV. THE HERMETIC WINDOW INDIUM-ALLOY SEAL

The hermetic seal is one of the challenges of scaling up MCP-PMTs in size. A solution consists of clamping the window in place on the tile base at a set gap width, typically 0.002", and 'wicking' molten indium alloy[41] into the gap by capillary action from wire placed contiguous to the gap[42]. The sealing surfaces require metalization prior to assembly. Both sealing surfaces are coated by evaporation with 200 nm of NiCr followed by 200 nm of Cu.

The tile base, inner amplification components, and window are clamped in place in a mechanical 'fixture' prior to the thermal sealing cycle. The fixture consists of a 0.50"-thick SS bottom plate that supports the tile base, a compression fixture to clamp the window onto the base from above, heating elements, and thermocouples for measuring the temperature during the process cycle. The copper tubulations are connected to the manifold to complete the inner vacuum system. Figure 7 shows an assembled tile in the fixture prior to sealing.

To bake out the tile and form the hermetic seal, two heating units, shown in Figure 7, consisting of 3mm-thick 6"-square ceramic plates wound with NiCr heating ribbon[43] are placed in thermal contact with the lower and and upper compression plates, as shown in Figure 7. The outer vacuum vessel is not heated.

Figure 8 shows the thermal cycle for Tile 31. The cycle consists of a ramp up of approximately 15 hours, a bake-out of 18 hours at 290 ^{o}C , followed by cool-down to room temperature. The feature around 220 ^{o}C is due to the formation of the indium alloy capillary seal.

Leak checking after sealing is performed in two steps. A global check is performed before opening the outer vacuum vessel using a Residual Gas Analyzer (RGA)[44] by back-filling the vessel with argon with the tile isolated from the UHV (inner) manifold. After several hours, the pump to the manifold is valved off, and the valve between the manifold and the tile is re-opened. The RGA can then detect through the manifold any argon accumulated in the tile. We estimate the sensitivity of the global check to be 1-2 10^{-13} mbar-liters/sec.

If a leak is detected, after the outer vessel is opened a systematic local search is performed with a helium leak detector[45] attached to the manifold and a needle probe helium source. We estimate the sensitivity of this local check to be several 10^{-11} mbar-liters/sec.

V. BAROIS PHOTO-CATHODE SYNTHESIS

The air-transfer assembly process involves depositing a Sb pre-cursor layer on the window prior to assembly. After the sealing cycle is complete and the tile is leak-tested, the tile is re-heated to a temperature of ≈120 ^{o}C , below the melting point of the solder seal, for photocathode synthesis by introducing alkali vapor[26,27].

The bialkali K_2CsSb photocathode cathode compound was synthesized directly as part of this program[22,23,46]. In the process development described here only a single alkali, Cs, was used for simplicity.

The cesium vapor source is shown schematically in Figure 9. A glass ampoule of Cs[47,48] is inserted in the vertical bellows section of the tee in the left-hand (ampoule) chamber. The ampoule is broken from above with a ceramic rod by compressing the bellows, as shown in Figure 9. The Cs liquid and glass ampoule can be observed through a sapphire window. The liquid Cs is then evaporated away from the glass shards of the ampoule into the right-hand (source) chamber by heating the ampoule chamber[49]. The valve between the source chamber and the ampoule chamber is then closed. A sapphire window in the source chamber allows visual monitoring of the surface of the distilled Cs. Cesiation of the tile is initiated by opening the valve to the manifold with the source chamber at 150-155 ^{o}C .

A 2-dimensional motion stage for mapping the photocathode response during photocathode synthesis is shown in Figure 10. The module is still connected to the UHV manifold; pinch-off occurs only after leak-checking and cathode characterization.

To measure the photo-response we applied a 37 V bias to the gap between the photocathode and the top surface of the first MCP. A 405 nm light-emitting diode was pulsed in phase with a lock-in amplifier and pico-ammeter to measure the current.

Figure 11 shows successive maps of the photo-response during the activation of the pre-cursor Sb layer by Cs vapor. The response grows to a saturation value near the inlet and then continues to the far side of the 8.26"-square window. The response saturates near 3% quantum efficiency (QE).

Neither the uniformity nor the end-point QE are satisfactory for a useable commercial device. We attribute the lower quantum efficiency near the edges to a non-uniform temperature of the window during synthesis. The tile was heated through its contact with the fixture lower plate, and was subject to convective cooling from above. Thermally isolating the assembly from convection should eliminate the non-uniform temperature of the window. In addition, the QE saturated, but

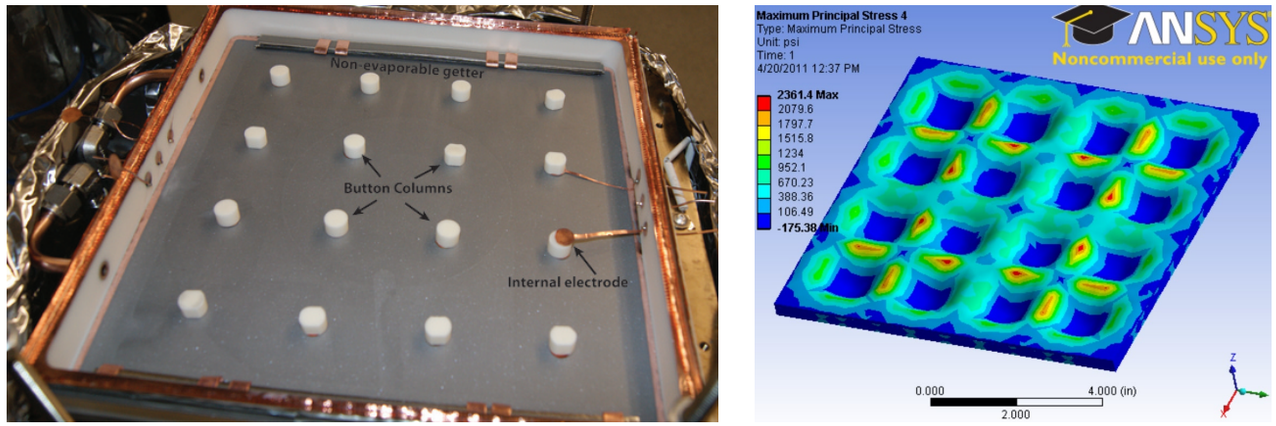

FIG. 6. Left:The tile base during assembly showing the spacer buttons and their connecting internal high-voltage electrodes. At the top of the picture the getter is positioned to be soldered to the NiCr anode layer during the bake-out thermal cycle. Right: A finite-element analysis of the stress on a B33 window under vacuum.

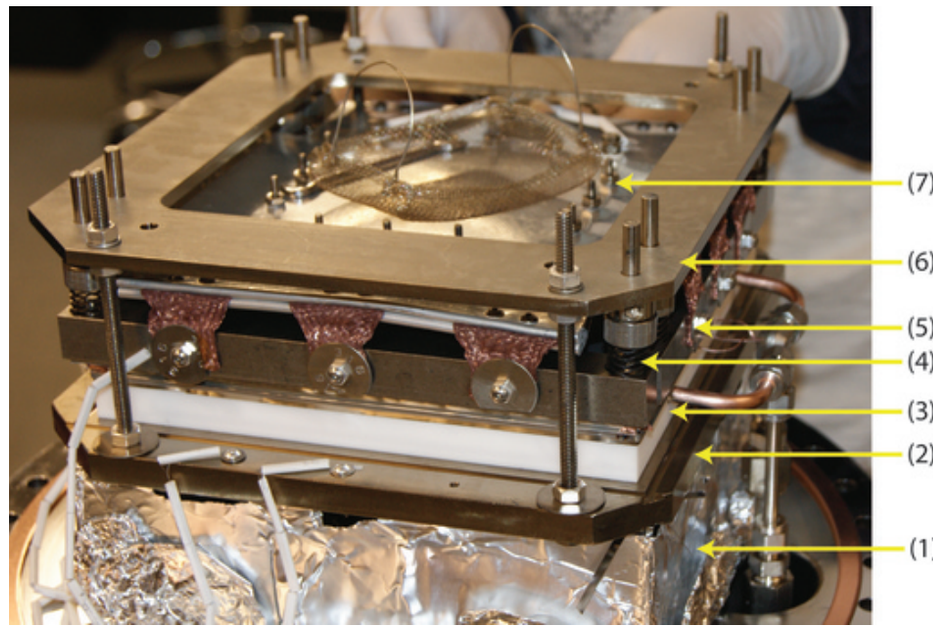

FIG. 7. An assembled tile clamped in place in the compression fixture prior to sealing. Heaters above and below the tile couple to the top and bottom fixture plates. The indicated components are: (1) the lower NiCr heater assembly; (2) the bottom compression fixture plate; (3) the tile assembly; (4) the compression mechanism; (5) floating rigid press bars; (6) the upper compression fixture plate; and (7) the upper NiCr heater assembly.

at a lower value than is attainable for a good Cs_3Sb cathode[50]. We attribute this to the overly-thick Sb precursor layer. The overall Cs vapor migration time through the tile in Fig.11 can be decreased by increasing the processing temperature.

Figure 12 shows that the micro-channel plates recover functionality after cesiation. There is an initial large drop in resistance that would preclude operation. After the alkali vapor is valved off, the plates increase in resistance, allowing operation after cooling with increased gain, but with high noise. The gain and noise then fall to operational values within a few hours.

After photocathode synthesis and characterization, the copper tubulations are hermetically sealed by pinching off[51]. The razor-sharp edge of the pinch is then potted for safety, and the tile can be removed from the fixture.

VI. CONCLUSIONS

Large-area MCP-based photomultipliers employing ALD coated plates have unique performance parameters, with typical gains greater than 10^7, amplification-section (as opposed to photocathode) noise less than a few Hz, sub-mm resolutions in each transverse spatial dimension, and time resolution

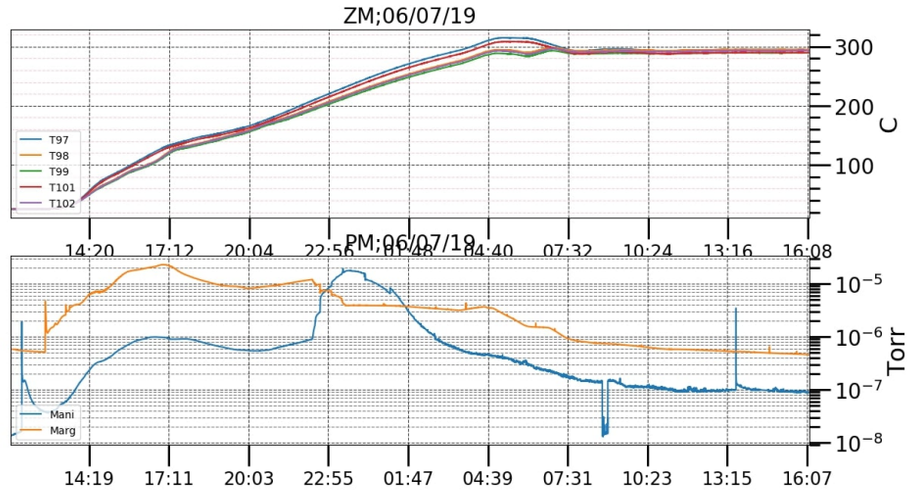

FIG. 8. The thermal cycle temperature and dual vacuum pressure data from Tile 31. The feature around 220 ^{o}C is due to the formation of the capillary seal between the two vacuum systems after the In-Ag alloy has melted at a temperature around 143 ^{o}C .

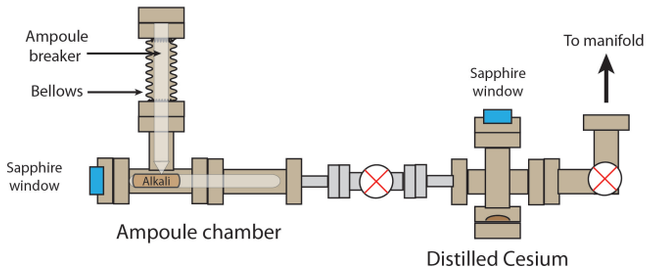

FIG. 9. Diagram of the alkali (Cesium) vapor source. The left-hand section is the ampoule chamber; the right-hand section is the source chamber.

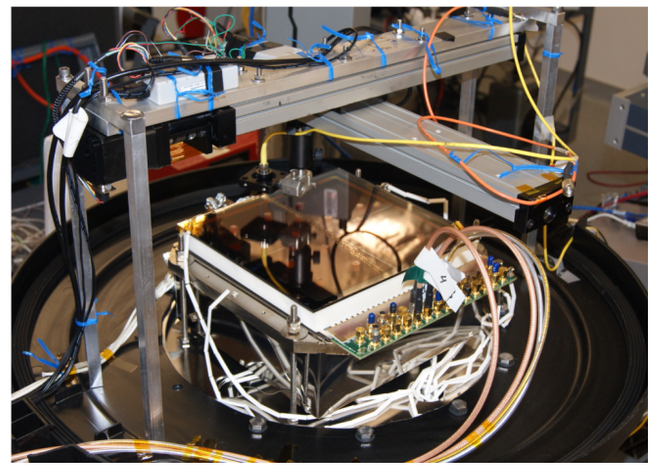

FIG. 10. A 2D scanning stage for mapping photo-response during and after photocathode synthesis.

of 5-10 psec for charged particles and 30-50 psec for single photons[40,52]. The small feature size, concomitant good resolutions, and high gain are intrinsic rather than highly tuned[9]. The ALD-based functionalization of the glass capillary substrates[36,37] eliminates the shortened tube lifetime due to ion feedback[1,53].

At the outset of this work the major obstacles to PMT-like batch production of large-area MCP-PMTs were identified as: a) the long and rectangular hermetic seal; b) 'in-situ' synthesis of alkali photo-cathodes in a large-area low-profile package; c) compromised performance of the MCPs after exposure to alkali vapors; and d) a robust package that supports large numbers of high bandwidth electrical signal connections to an external readout system. We address these in turn below.

The demonstrated solution to the hermetic seal relies on: a) clamping the window at the pre-set width of the solder seal layer prior to heating; clean Au or Cu surfaces on the window and base with no solder material (and hence no oxides) in the gap prior to sealing; b) allowing capillary action to 'wick' the molten alloy into the window-base gap during bakeout away from oxide; and c) use of In-Ag alloy as solder.

After this work started, we discovered that the chemistry of the 'in-situ' photo-cathode synthesis starting with a pre-deposited uniform thickness Sb layer was studied in depth 30 years ago[26,27]. We also discovered that the air transfer of the window with a pre-deposited Sb layer is currently in use commercially[28]. We note that Ref.[27] states "Manufacturing photo-emissive layers by equilibrating the antimonides with binary alkali vapors would lead to a product with a better definition than those obtained through the dynamic process used at present".

The recovery of MgO-coated MCP functionality after exposure to Cs vapor during photocathode synthesis was demonstrated. The plates initially drop dramatically in resistance, and both gain and noise increased, but recover with subsequent operation before pinch-off.

Lastly, the development of capacitive coupling of an internal thin metal anode layer to an external, application-specific, signal-pickup printed circuit board enables the decoupling of

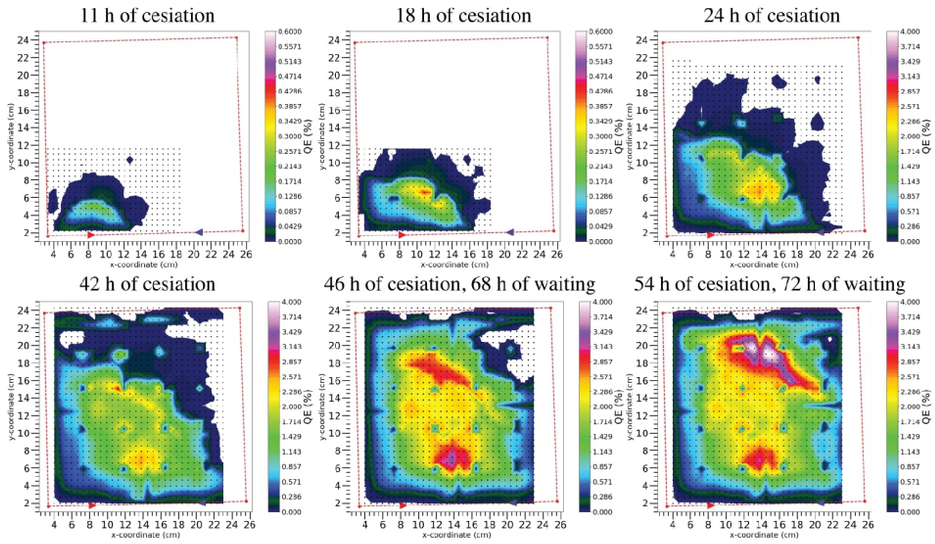

FIG. 11. Successive maps of the photo-response for Tile 31 during photocathode synthesis.

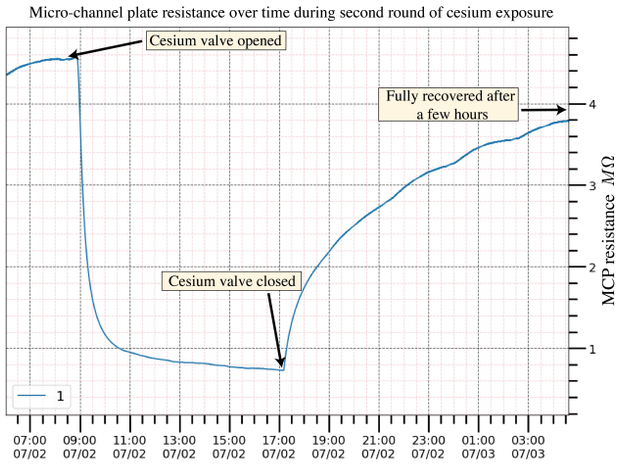

FIG. 12. The resistance of the stack of two microchannel plates and spacers during a cesiation cycle, showing that the plates recover functionality after an initial large drop in resistance.

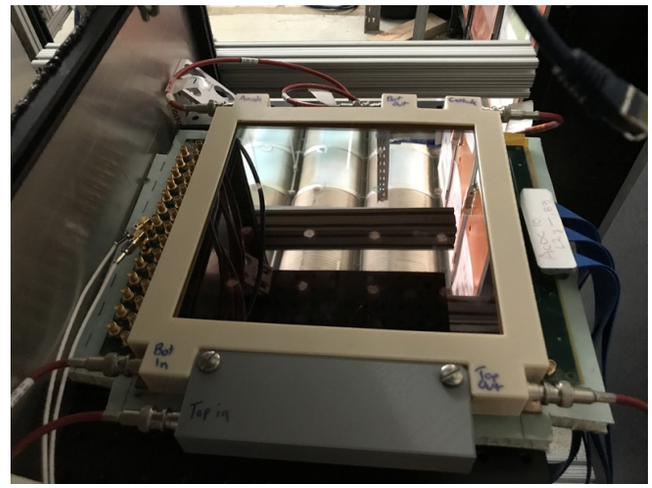

FIG. 13. The UC LAPPD^{TM} Tile 31 with a signal readout board and HV connections.

the photomodule design from the optimization of pads or strips for high-bandwidth signals for applications requiring many pads or strips in the readout[31].

We have shown that each of these potential 'show-stopper' obstacles is technical rather than fundamental. A proof-of principle solution to each that is scalable to batch production is described above. However, the development of an optimized industrial batch process for bringing volume up and cost down for wide-spread use in particle physics, medical imaging, and nuclear security remains as the task for commercialization.

VII. ACKNOWLEDGEMENTS

The University of Chicago is supported by the HEP Division of the Department of Energy under con tract DE-SC-0008172 and DE-SC-0020078, by the National Science Foundation under grant PHY-106601 4, and by the Physical Sciences Division of the University. The development at Incom is supported by the DOE Nuclear Physics Division through award number DE-SC0015267.

The data that support the findings of this study are available from the corresponding author upon reasonable request.

The authors hold three patents related to this work[19,20,42].

We thank the many collaborators and experts who have contributed. Special thanks for critical interventions are due to Oswald Siegmund, Anton Tremsin, Jason McPhate, Howard

Nicholson, Klaus Attenkofer, Sergey Belyanchenko (MELZ), Howard Clausing (Clausing LLC), Jeffrey DeFazio (Photonis), Igor Fedorov (MELZ), Mary Heintz, Giles Humpston, Robert Jarrett (Indium Corp.), Christine Mariano (International Ceramics Engineering), Helmut Marsiske, Rich Northrop, Matthew Poelker, Charles Sinclair, and Neal Sullivan (Arradiance).

[1] J. Anderson et al., *The Development of Large Area Photodetectors*, proposal to the DOE; April 22, 2009; `http://psec.uchicago.edu/other/LAPPD_DOE_Proposal.pdf`

[2] E. Angelico, J. Eisch, A. Elagin, H. J. Frisch, S. Nagaitsev, M. Wetstein; *Energy and Flavor Discrimination Using Precision Time Structure in On-Axis Neutrino Beams*, Phys. Rev. D, 100, 032008 (Aug. 2019); arXiv:1904.01611

[3] E. Oberla and H.J. Frisch; *Charged particle tracking in a water Cherenkov optical time-projection chamber*; Nucl. Inst. Meth. Phys. Res. A814, 19 (April 2016); ISSN 0168-9002; arXiv:1510.00947

[4] A. Elagin, H. J. Frisch, B. Naranjo, J. Ouellet, L. Winslow, T. Wongjirad; *Separating Double-Beta Decay Events from Solar Neutrino Interactions in a Kiloton-Scale Liquid Scintillator Detector By Fast Timing* Nucl. Inst. Meth. Phys. Res. A. (Sept. 2016);

[5] C. Aberle, A. Elagin, H.J. Frisch, M. Wetstein, L. Winslow; *Measuring Directionality in Double-Beta Decay and Neutrino Interactions with Kiloton-Scale Scintillation Detectors*; Journal of Instr., Volume 9 (June 2014) JINST 9 P06012 doi:10.1088/1748-0221/9/06/P06012 e-Print arXiv:1307.5813

[6] E. Spieglan; *Using Switchable Fluorescent Molecules to Image Tracks and Measure Energy in Large Liquid Double Beta Decay Detectors*; CPAD 2019; `https://agenda.hep.wisc.edu/event/1391/timetable/#20191209.detailed`

[7] A. Li, A. Elagin, S. Fraker, C. Grant, and L. Winslow; *Suppression of Cosmic Muon Spallation Backgrounds in Liquid Scintillator Detectors Using Convolutional Neural Networks*; Nucl. Instr. Meth. Phys. Res. A947 (2019) 162604

[8] J. Gruszko, B. Naranjo, B. Daniel, A. Elagin, D. Gooding, C. Grant, J. Ouellet and L. Winslow, *Detecting Cherenkov light from 1–2 MeV electrons in linear alkylbenzene*; JINST 14 (2019) no.02, P02005

[9] H. J. Frisch; *Drifting Photons on Optical Paths, Mirrors, Sub-mm Resolution in Four Dimensions, and Transverse/Longitudinal Phase Space: Exploiting Psec Time Resolution*; Proceedings of the 5th International Conference on Micro-Pattern Gas Detectors (MPGD2017); 22-26 May, 2017, Philadelphia, USA; Proceedings in Science, 2018

[10] Y. Wah (KOTO Collaboration), private communication.

[11] C. Corrado (REDTOP Collaboration); *The REDTOP experiment*; Talk presented at DPF2019, July, 2019; Boston; `https://arxiv.org/pdf/1910.08505.pdf`

[12] H. Kim, H. J. Frisch, C.-M. Kao, Q. Xie, C.-T. Chen, L. Zhou, F. Tang, W.W. Moses, W.S. Choong; *A Multi-Threshold Sampling; Method for TOF PET Signal Processing*; Nucl. Inst. and Meth. A602, 618, 2009.

[13] H. Kim, H. J. Frisch, C.-T. Chen J.-F. Genat, F. Tang, W.W. Moses, W. S. Choong, and C.-M. Kao; *A Design of a PET Detector Using Micro-Channel Plate Photo-Multipliers with Transmission-Line Readout*; Nucl. Inst. and Meth. A622, p628 (2010)

[14] H. Kim, H. J. Frisch, C.-T. Chen J.-F. Genat, F. Tang, W.W. Moses, W. S. Choong, and C.-M. Kao; *A Prototype TOF PET Detector Module Using a Micro-Channel Plate Photomultiplier Tube with Waveform Sampling*; Nucl. Instr. and Meth. A662 (2012) 26-32

[15] H. J. Frisch, E. J. Oberla, H.-J. Kim, M. Yeh, U.S. Patent 10,132,94, Nov., 2018

[16] M. Askins et al. (Watchman Collaboration); *The Physics and Nuclear Nonproliferation Goals of WATCHMAN: A WAter CHerenkov Monitor for ANtineutrinos*; https://arxiv.org/abs/1502.01132

[17] Photonis/Burle Industries, 1000 New Holland Ave., Lancaster PA, 17601. We are grateful for the hospitality and advice during several visits to the plant.

[18] B. Adams et al.; *A Brief Technical History of the Large-Area Picosecond Photodetector (LAPPD) Collaboration*; ArXiV:1603.01843

[19] H. Frisch, M. Wetstein, A. Elagin, *Batch Production of Microchannel Plate Photo-Multipliers*, Patent No. US9911584B2, 2017, `https://patents.google.com/patent/US9911584B2`

[20] H. J. Frisch, E. Angelico, A. Elagin, E. Spieglan, and B. W. Adams; *Dual Low Vacuum-UltraHigh Vacuum System for Large-Scale Production of Micro-Channel Plate Photomultipliers*; US Patent 62928598

[21] . C. Sinclair; discussion at *First Workshop on Photocathodes: 300nm-500nm*; Univ. of Chicago, Chicago, IL; July 2009; https://psec.uchicago.edu/workshops/photocathodeConference/talks/

[22] V/ Nagarkar. H. Bhandari, (RMD Inc), K. Attenkofer, H.J. Frisch, and J. Smedley; *Theory-Based High-QE Photocathode Development*; DOE SBIR DE-SC0009540

[23] H. Bhandari, (RMD Inc), L. Cultrera, J. DeFazio, and J. Smedley; *Manufacturing and Packaging of Reliable Bialkali Photocathodes via Sputtering* DOE SBIR DE-SC0017202; May, 2018

[24] J. Smedley et al., *Sputter Growth of Alkali Antimonide Photocathodes: An In Operando Materials Analysis*; Proceedings of IPAC2015, May 2015; Richmond VA TUPHA003

[25] M. Gaowei, Z. Ding, S. Schubert, H. B. Bhandari, J. Sinsheimer, J. Kuehn, V. V. Nagarkar, M. S. J. Marshall, J. Walsh, E. M. Muller, K. Attenkofer, H. J. Frisch, H. Padmore, and J. Smedley; *Synthesis and x-ray characterization of sputtered bi-alkali antimonide photocathodes*; APL Materials 5, 116104 (2017); https://doi.org/10.1063/1.5010950

[26] B. Tanguy, J. M. Barois and M. Onillon; *Experimental Study of the Equilibria of Cesium Potassium Antimonides with Alkali Vapours*; Materials Chemistry and Physics, 30 (1991) 7-12;

[27] J. M. Barois, C. F., M. Onillon. and B. Tanguy; *Experimental Study of the Non-Stoichiometry of Cesium Antimonide: Cs_3Sb*; Materials Chemistry and Physics, 24 (1989) 189-197

[28] MELZ–FEU Ltd; Zelenograd, Russia; www.melz-feu.ru; PMT catalog number FEU-527

[29] Thierry Gys and Christian Joram; *Position-sensitive vacuum photon detectors* Nucl. Instr. Meth. A (Jan. 2020), 163373

[30] "*Manufacturing photoemissive layers by equilibrating the antimonides with binary alkali vapors would lead to a product with a better definition than those obtained through the dynamic process used at present*"; B. Tanguy et al (op. cit)

[31] E. Angelico, T. Seiss, B.W. Adams, A. Elagin, H. Frisch, E. Oberla, E. Spieglan; *Capacitively coupled Pulse Readout in a 20cm×20cm MCP-based photodetector* Nucl. Instr. Meth. A, 2016

[32] Typically 99.8% purity. Components were assembled using ceramic bases from International Ceramics Engineering (Worcester MA) and Friatec (Aliaxis), Mannheim, de.

[33] For details see Images 304, 315,316 and 320 at `http://image-library.uchicago.edu/`

[34] SAES getter St707/CTS/NI/8. Six strips each 8" long provided a total of 7.6 grams of St707. See `https://www.saesgetters.com/sites/default/files/St%20707%20Strips_0.pdf`

[35] H. L. Clausing Inc, Skokie IL

[36] The glass capillary substrates are manufactured by Incom Inc., Charlton Mass. See http://www.incomusa.com/

[37] Minot M. J., et. al. *Large area picosecond photodetector (LAPPD^{TM}) offers fast timing for nuclear physics and medical imaging*, Submitted for publication in "Il Nuovo Cimento" January 9, 2020

[38] The microchannel plates used in Tile 31 were functionalized with ALD by Arradiance, LLC; Littleton MA

[39] F. Tang, C. Ertley, J.-F. Genat, J. Anderson, K. Byrum, G. Drake, E. May, and G. Sellberg *Transmission-Line Readout with Good Time and Space Resolutions for Planacon MCP-PMTs*; Topical Workshop on Electronics for Particle Physics, CERN, pp. 579-583, 2008

[40] B. Adams, M. Chollet, A. Elagin, A. Vostrikov, M. Wetstein, R. Obaid, and P. Webster *A Test-facility for Large-Area Microchannel Plate Detector Assemblies using a Pulsed Sub-picosecond Laser* Review of Scientific Instruments **84**, 061301 (2013)

[41] Indium/Silver (97/3.0) eutectic solder wire; Indium Wire Extrusion Inc., Durango, CO 81301. The quoted melting point is 143^{o}C .

[42] H. J. Frisch, E. Angelico, A. Elagin, and E. Spieglan; *Methods of Fabricating Vacuum Housing with Hermetic Solder Seals Using Capillary Wicks*; US Patent 62/831.474 (Pending)

[43] E. Spieglan, PSEC Document Library #349; http://lappddocs.uchicago.edu/

[44] Stanford Research Systems Model RGA200/12

[45] Pfeiffer Model ASM340
[46] H. Bhandari, V. Nagarkar, O. Ovechkina, H. J. Frisch, K. Attenkofer and J. Smedley; *Alkali Semi-Metal Films and Method and Apparatus for Fabricating Them* US Patent 14/884,947; Jan. 2015 (Pending)
[47] Alfa Aesar (Thermo Fisher Scientific); Ward Hill, MA
[48] ESPI Metals; Ashland, Oregon 97520
[49] During distillation the ampoule chamber is heated to 240 ^{o}C and the source chamber to 210 ^{o}C .
[50] L. Cultrera, H. Lee, I.V. Bazarov, *Alkali antimonides photocathode growth using pure metals evaporation from effusion cells*; Journal of Vacuum Science and Technology B34, 011202, (2016)
[51] HY-250 Hydraulic Pinch Tool; Custom Products & Services, Inver Grove Heights, MN
[52] B.W. Adams, A. Elagin, H. Frisch, R. Obaid, E. Oberla, A. Vostrikov, R. Wagner, J. Wang, M. Wetstein; *Timing Characteristics of Large Area Picosecond Photodetectors*; Nucl. Inst. Meth. Phys. Res. A. , Vol. 795, 1 (Sept. 2015).
[53] A. Lehmann et al.; *Lifetime of MCP-PMTs and other performance features*; Journal of Instrumentation, Vol. 13, February 2018

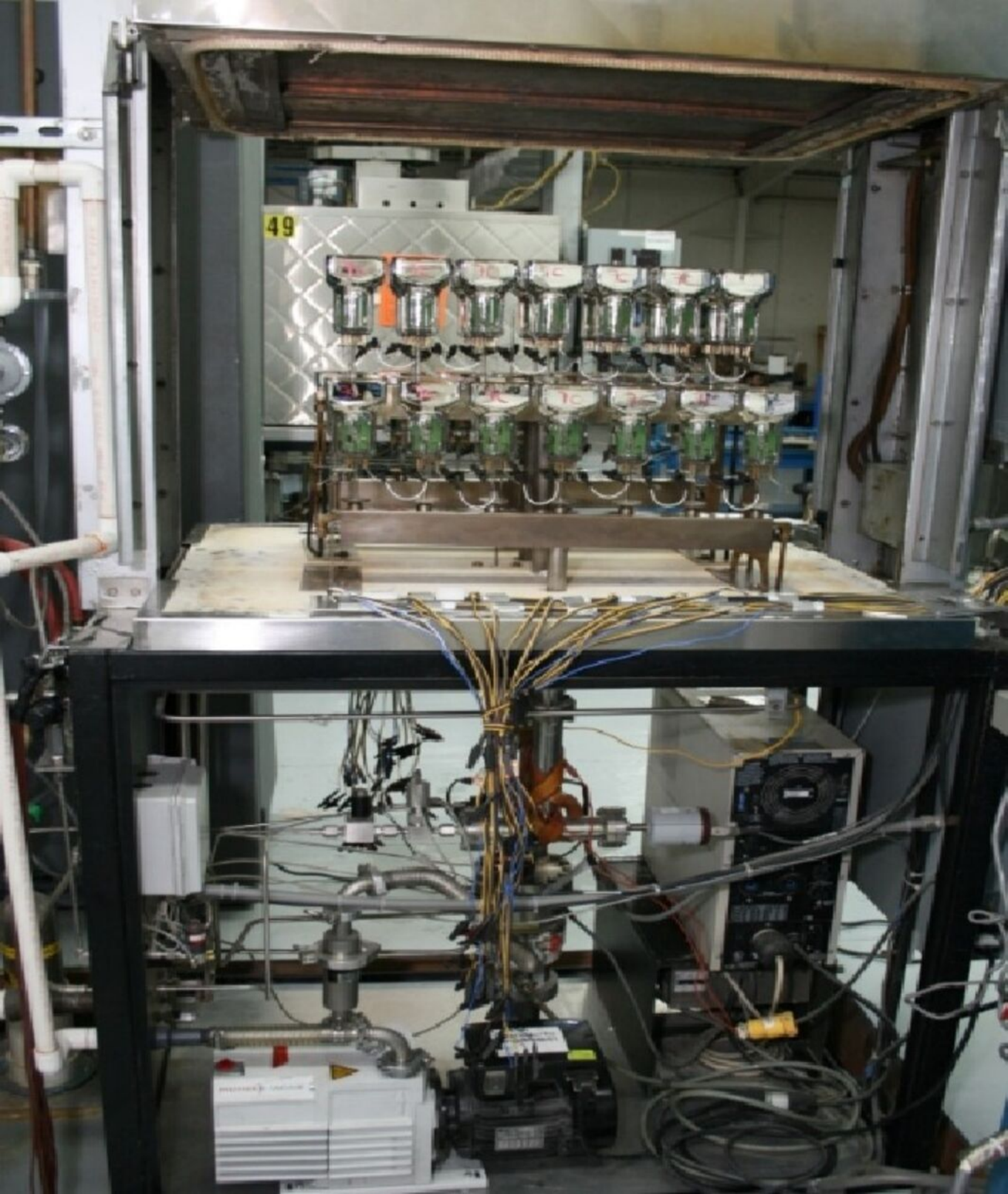
49

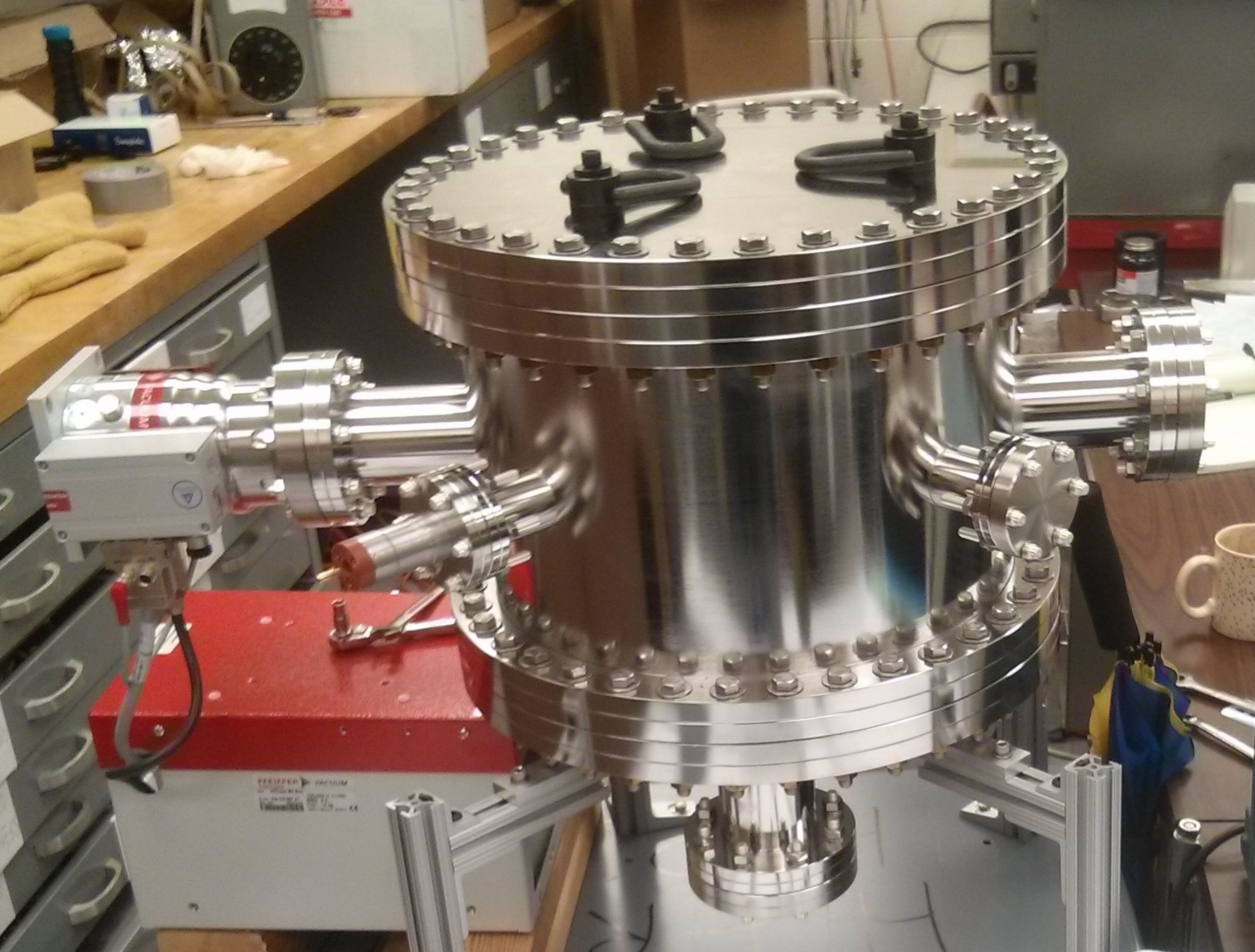

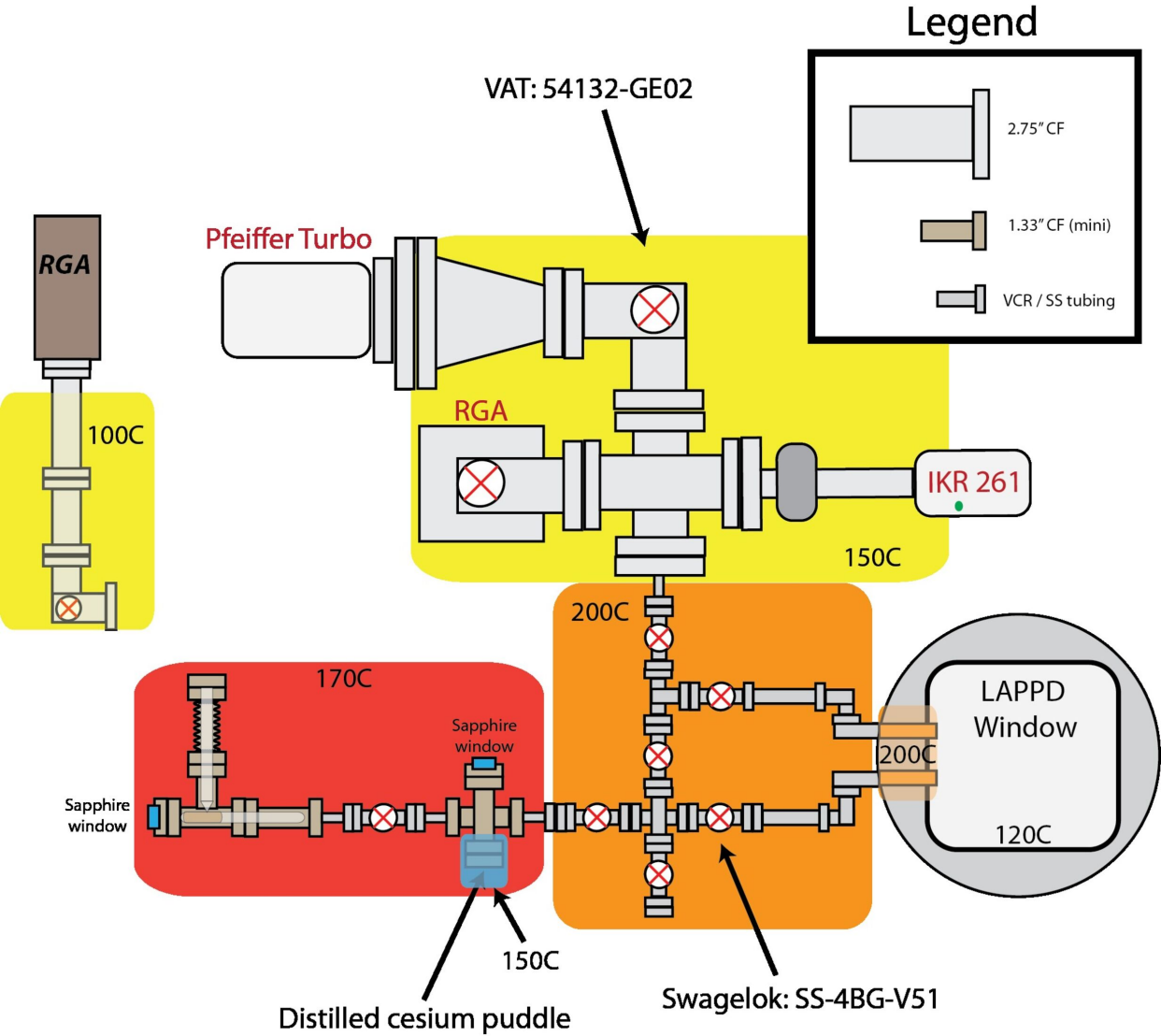
Legend
2.75" CF
1.33" CF (mini)
VCR / SS tubing
VAT: 54132-GE02
Pfeiffer Turbo
RGA
100C
RGA
IKR 261
150C
200C
170C
Sapphire window
Sapphire window
200C
LAPPD Window
120C
150C
Distilled cesium puddle
Swagelok: SS-4BG-V51

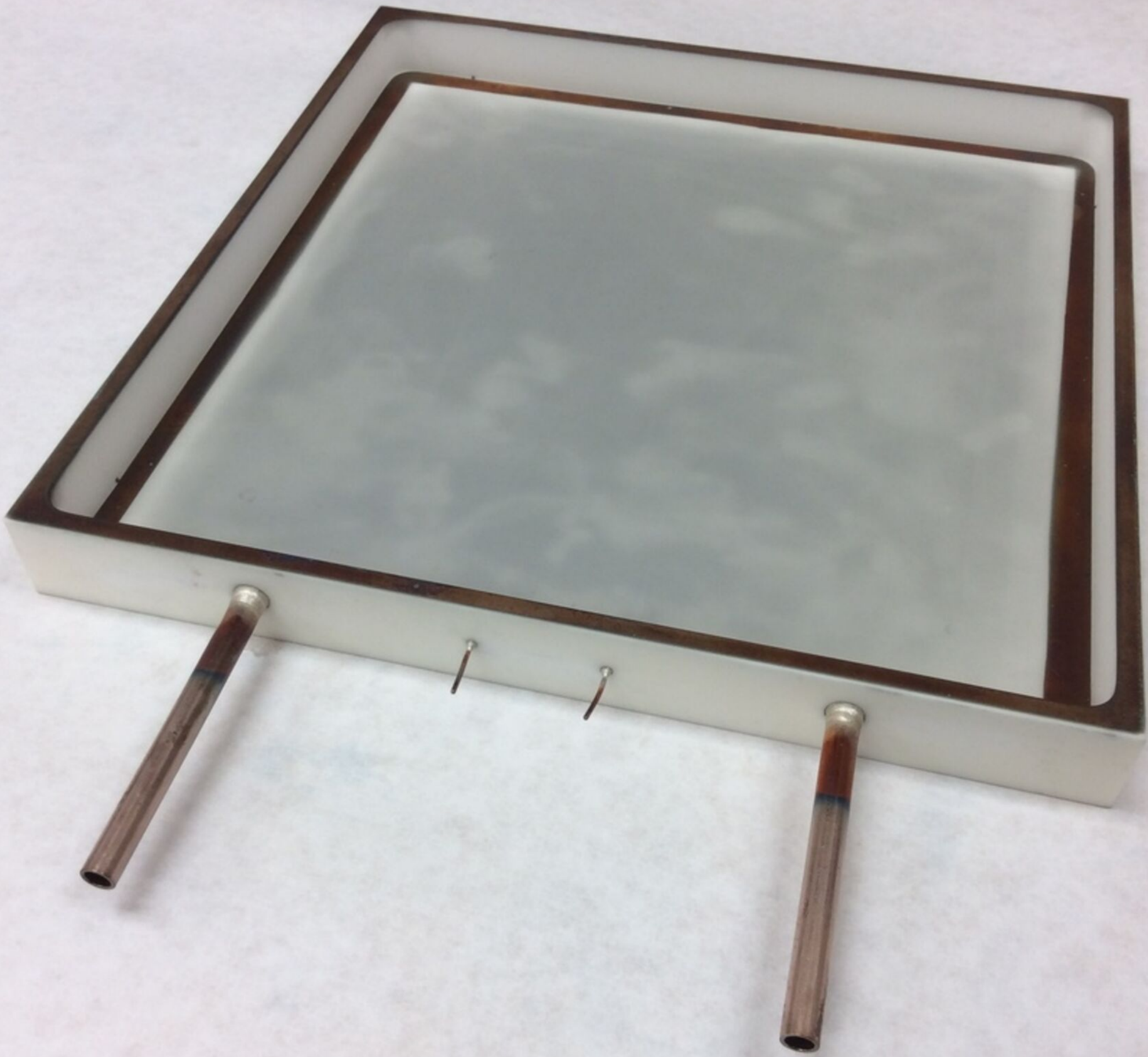

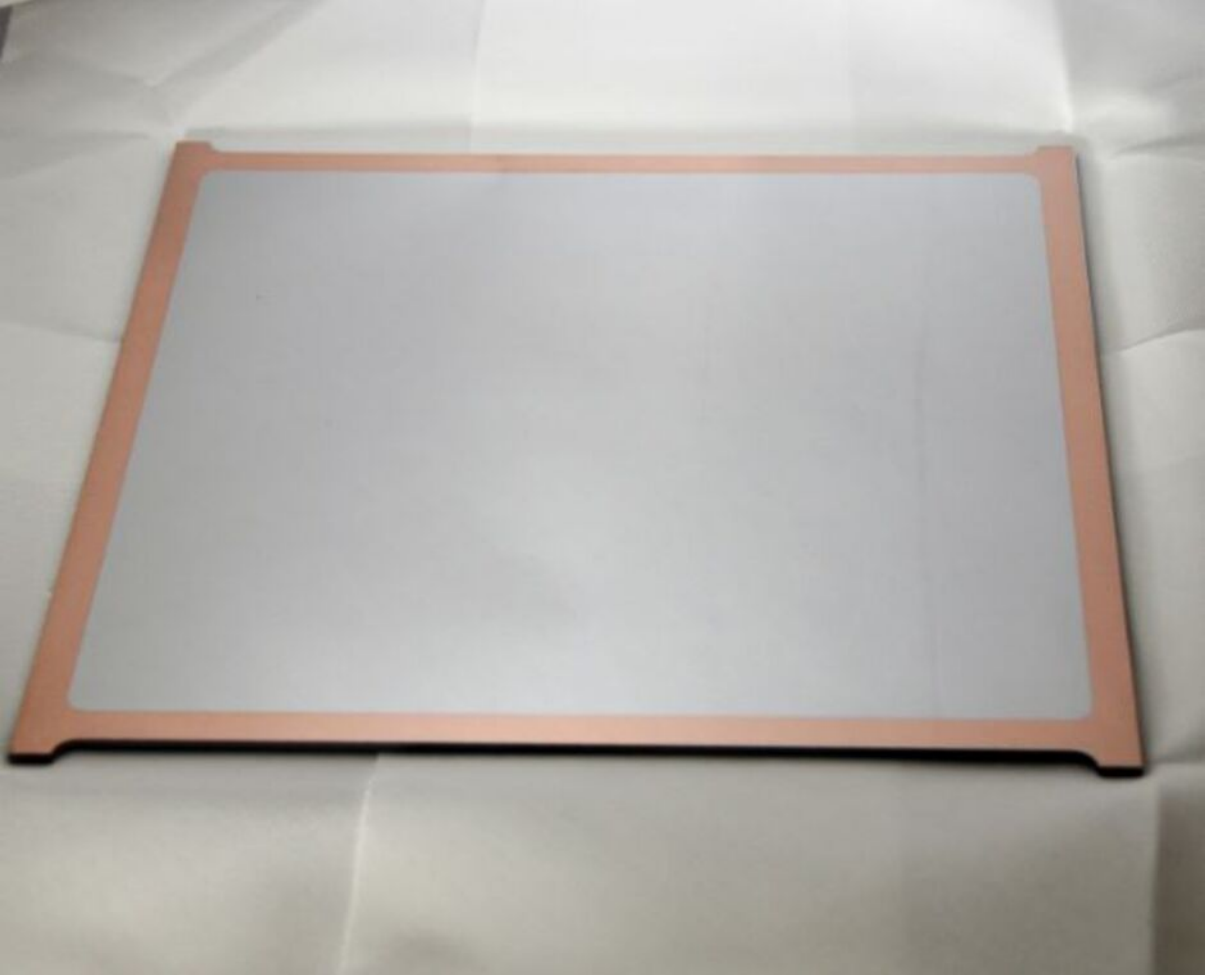

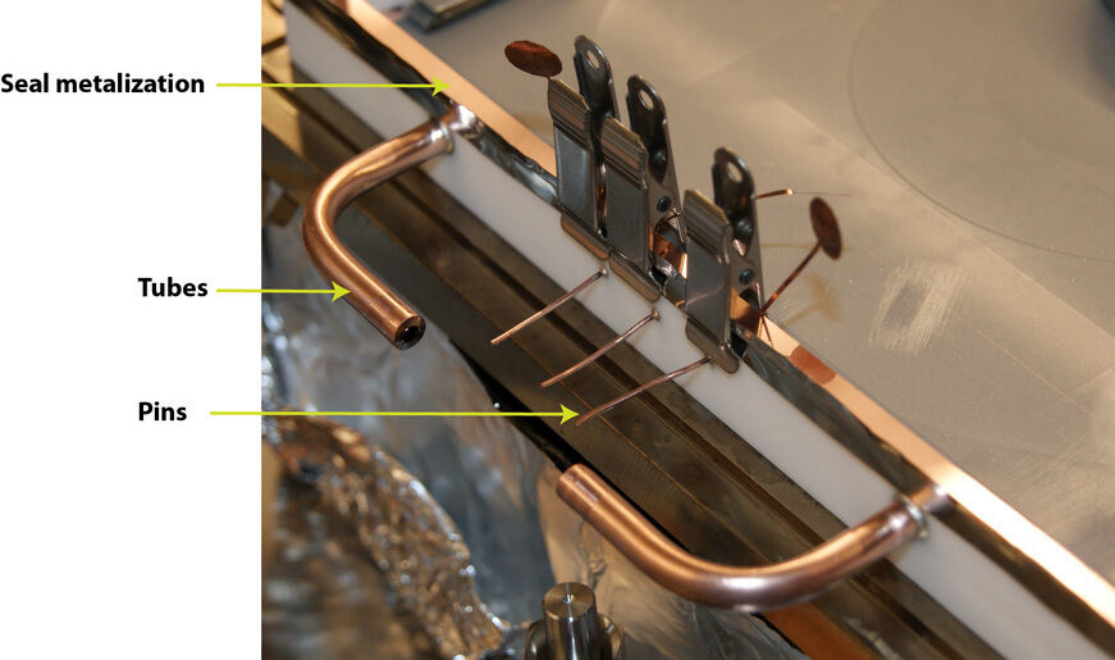
Seal metalization
Tubes
Pins

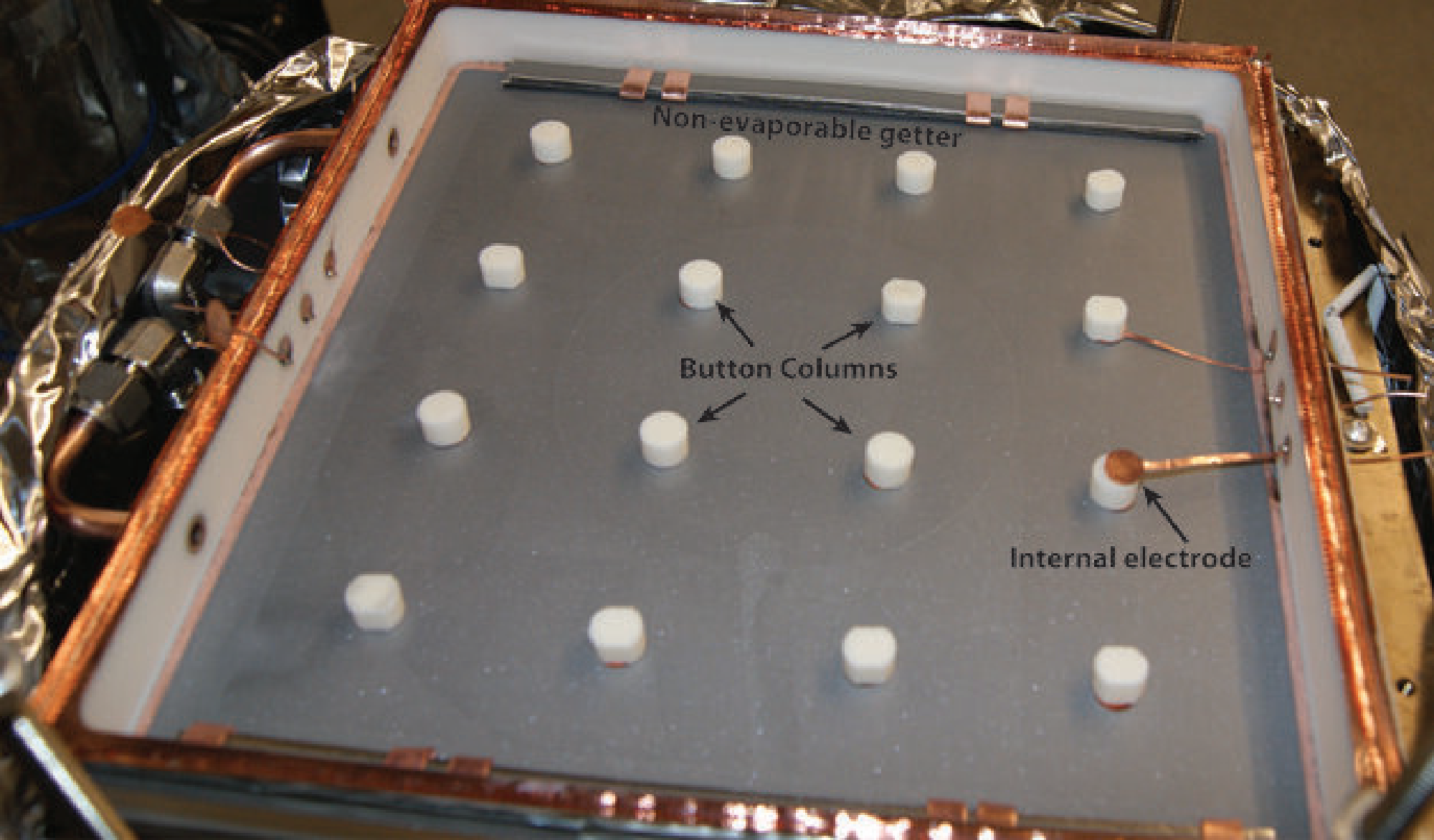
Non-evaporable getter
Button Columns
Internal electrode

Maximum Principal Stress 4
Type: Maximum Principal Stress
Unit: psi
Time: 1
4/20/2011 12:37 PM

2361.4 Max
2079.6
1797.7
1515.8
1234
952.1
670.23
388.36
106.49
-175.38 Min

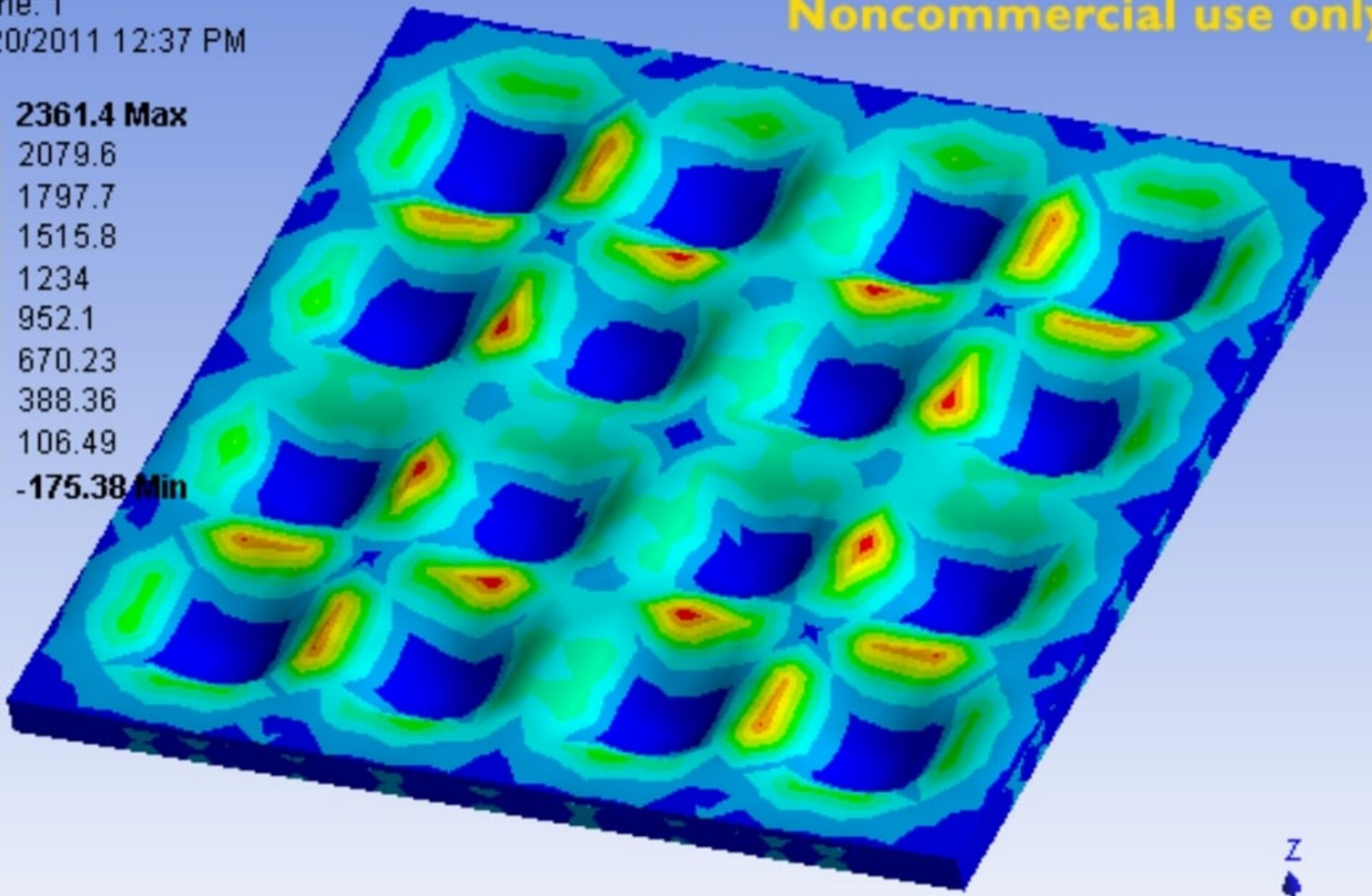

0.000 4.000 (in)
2.000

Z
X

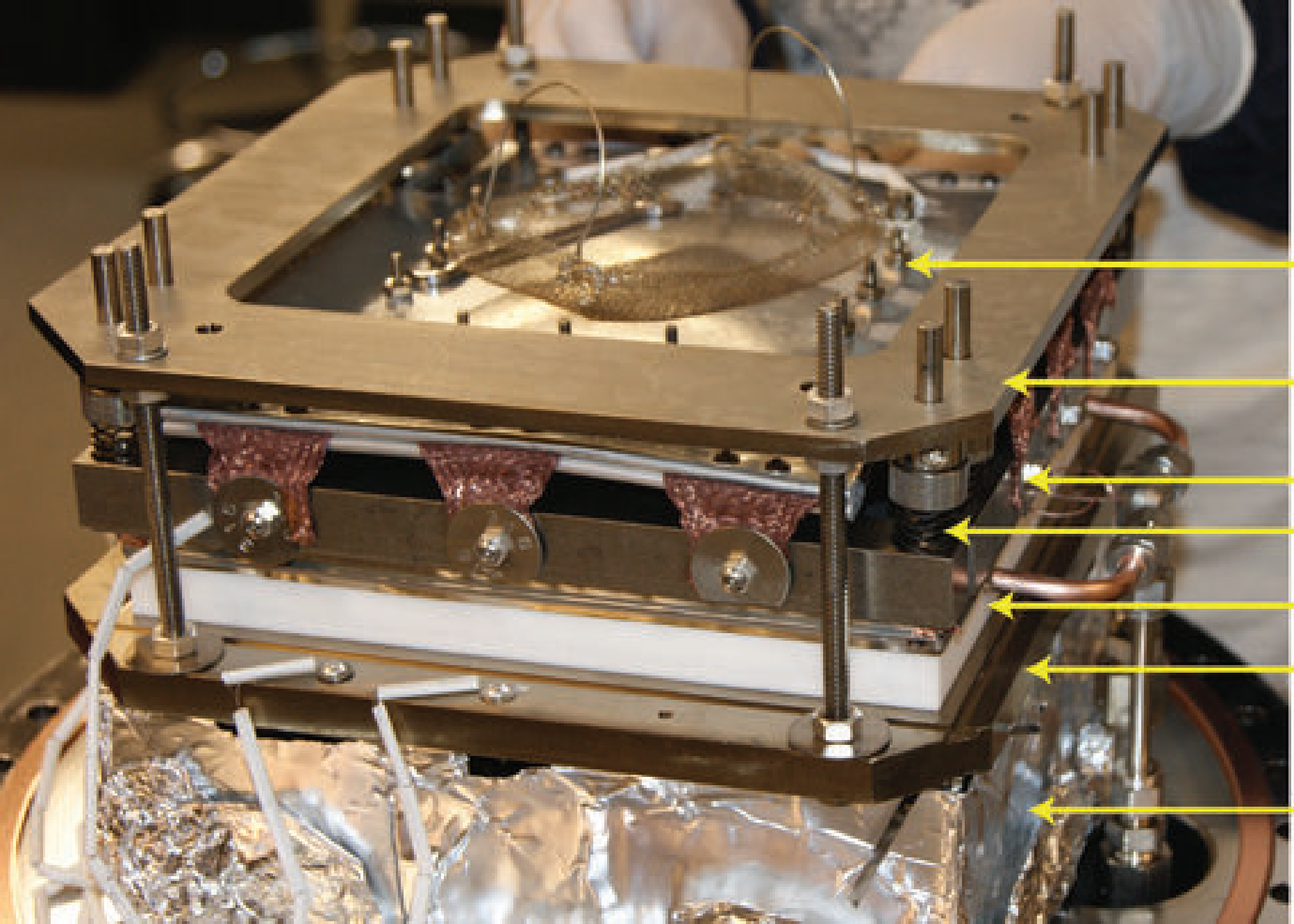
(7)
(6)
(5)
(4)
(3)
(2)
(1)

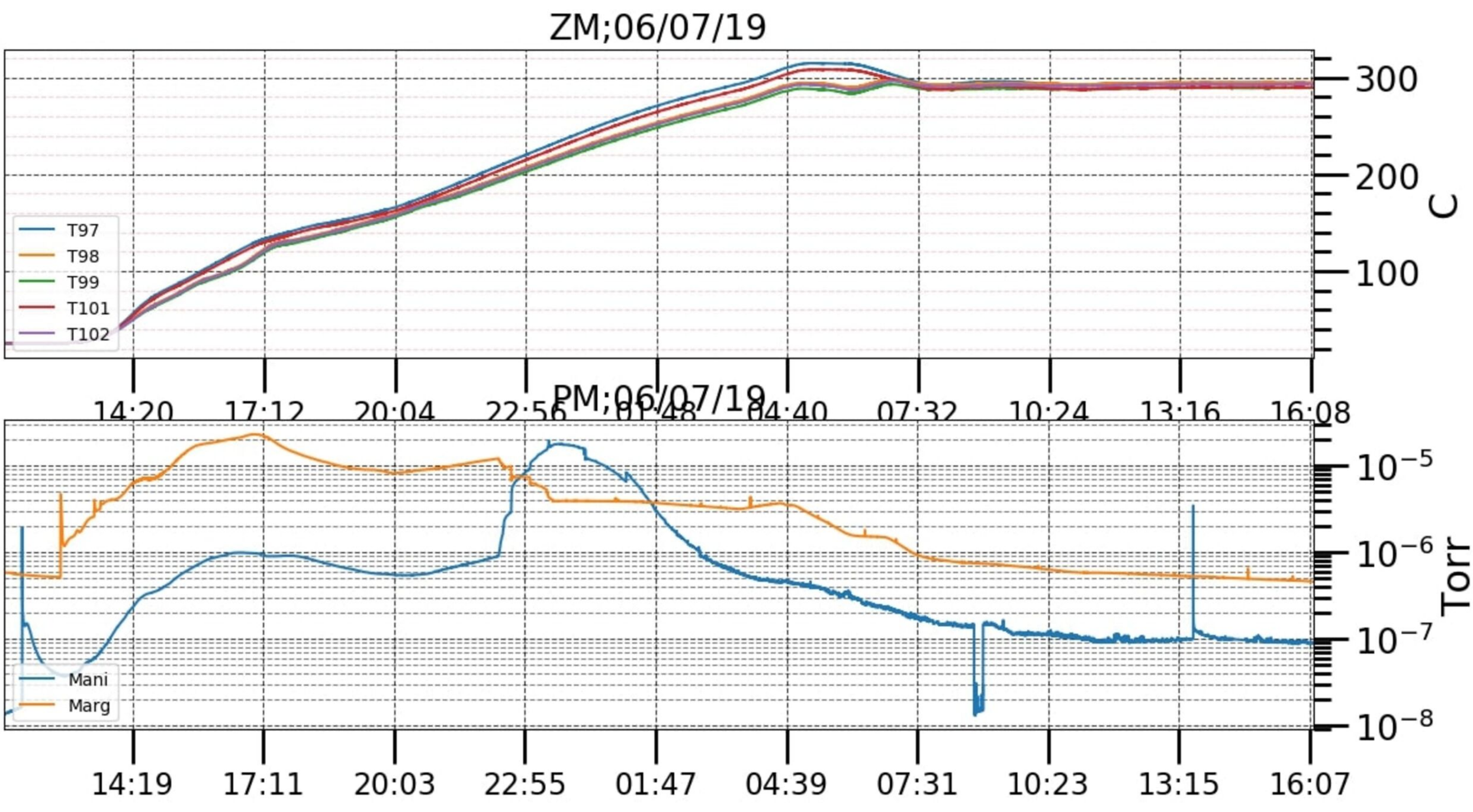
ZM;06/07/19
T97
T98
T99
T101
T102
300
200
100
C
14:20
17:12
20:04
22:56
01:48
04:40
07:32
10:24
13:16
16:08
PM;06/07/19
Mani
Marg
10^{-5}
10^{-6}
10^{-7}
10^{-8}
Torr
14:19
17:11
20:03
22:55
01:47
04:39
07:31
10:23
13:15
16:07

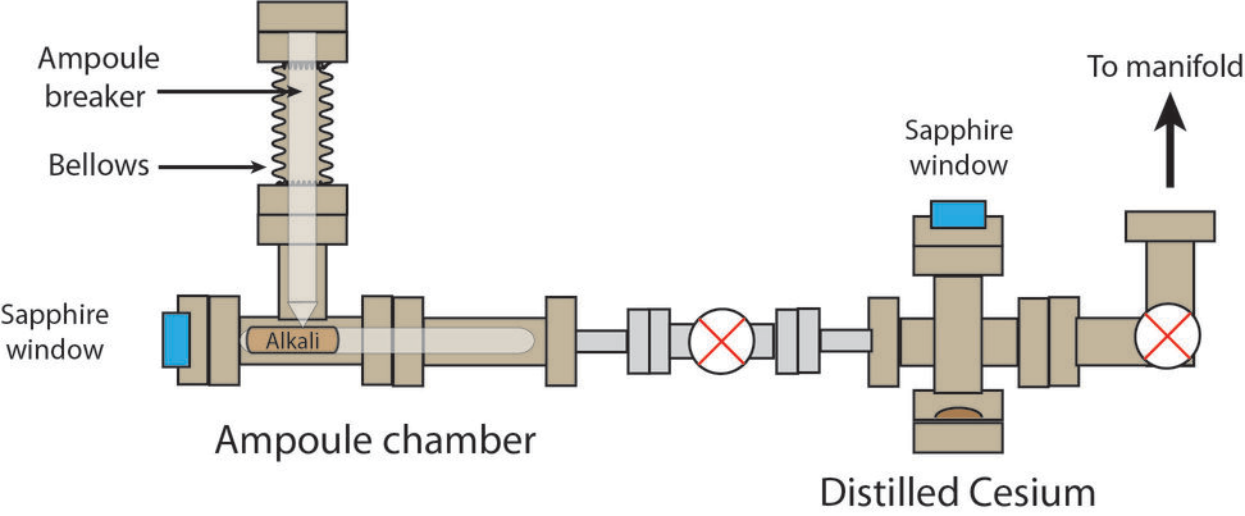
Ampoule
breaker
Bellows
Sapphire
window
Alkali
Ampoule chamber
Sapphire
window
To manifold
Distilled Cesium

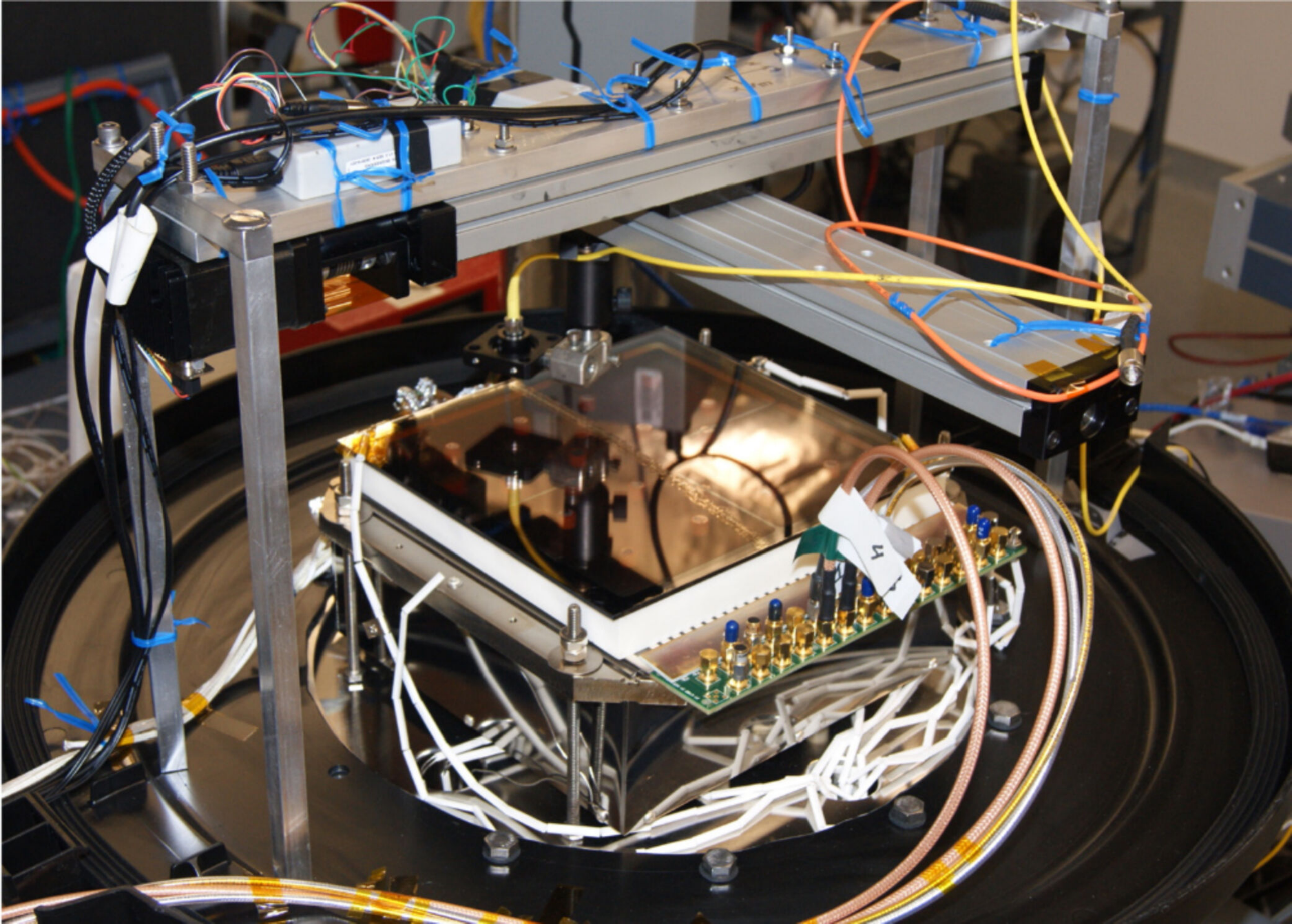

11 h of cesiation

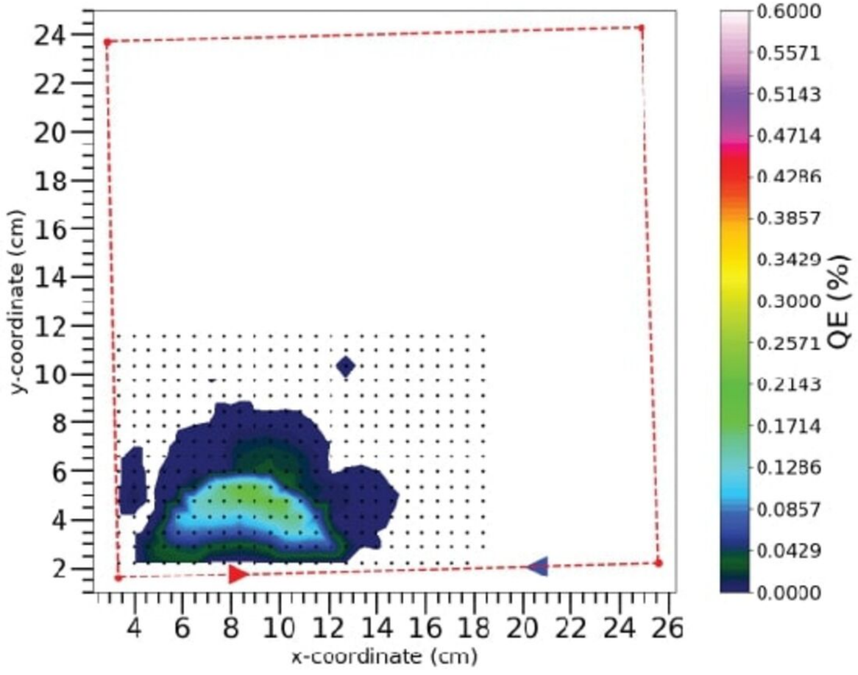

18 h of cesiation

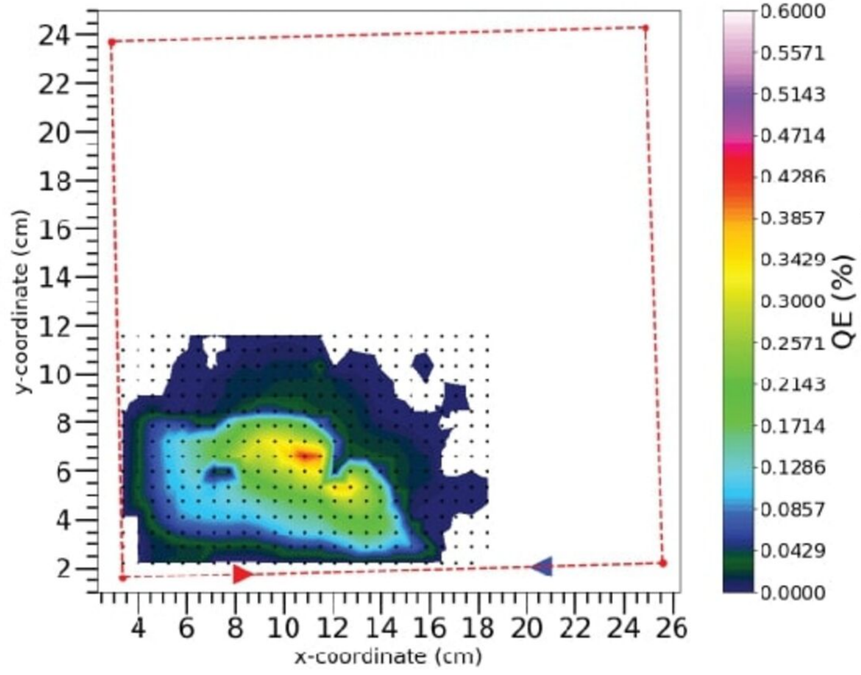

24 h of cesiation

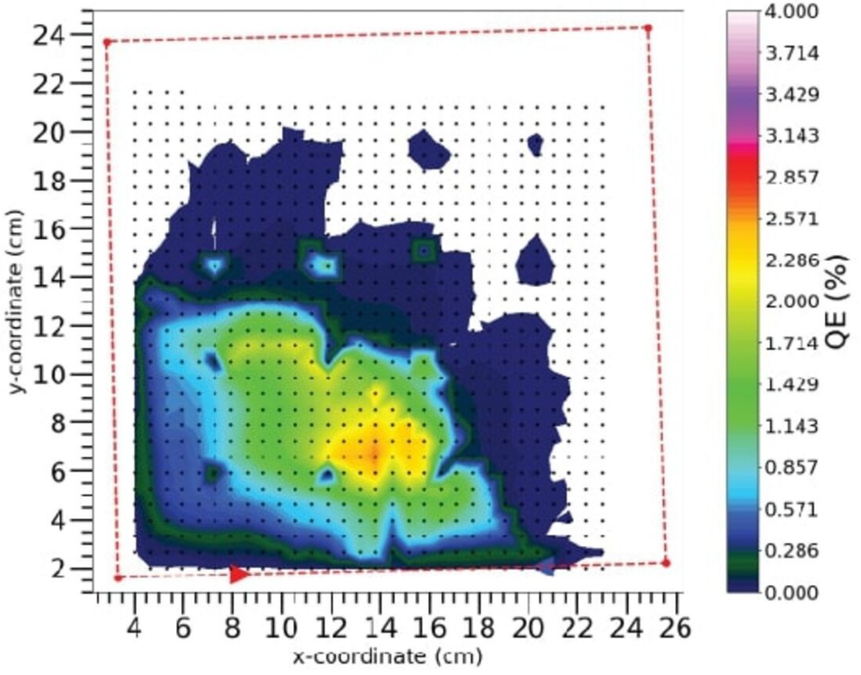

42 h of cesiation

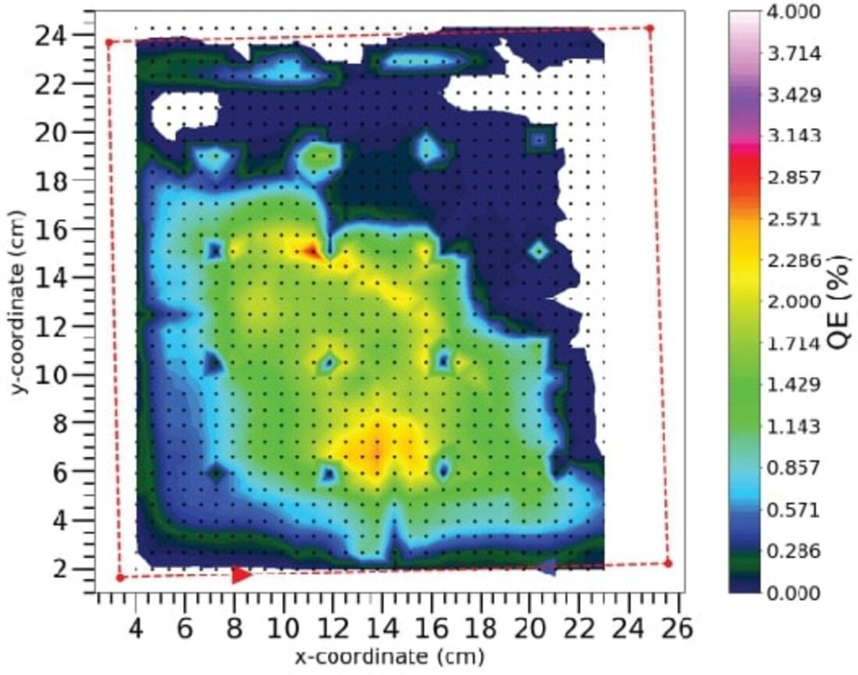

46 h of cesiation, 68 h of waiting

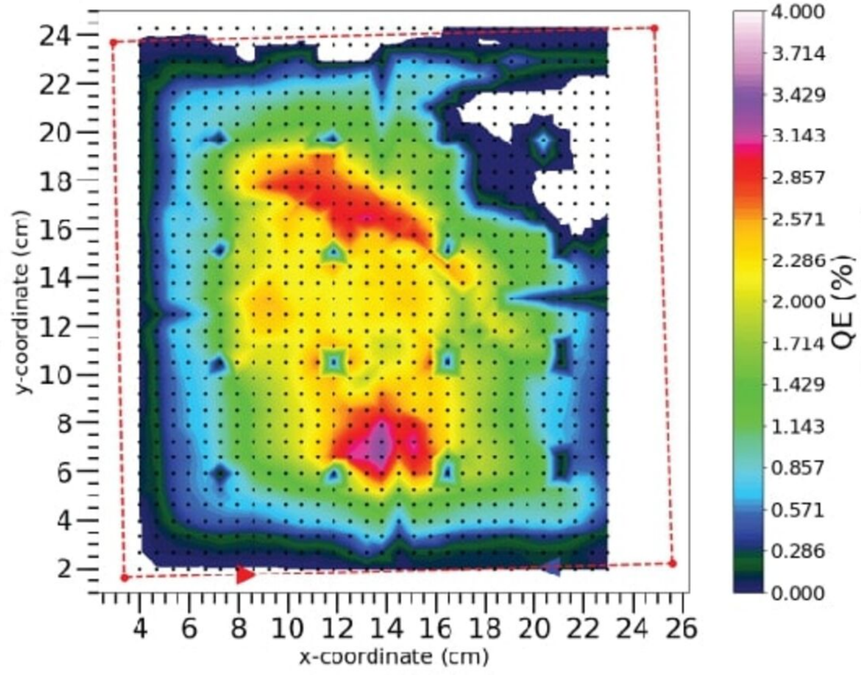

54 h of cesiation, 72 h of waiting

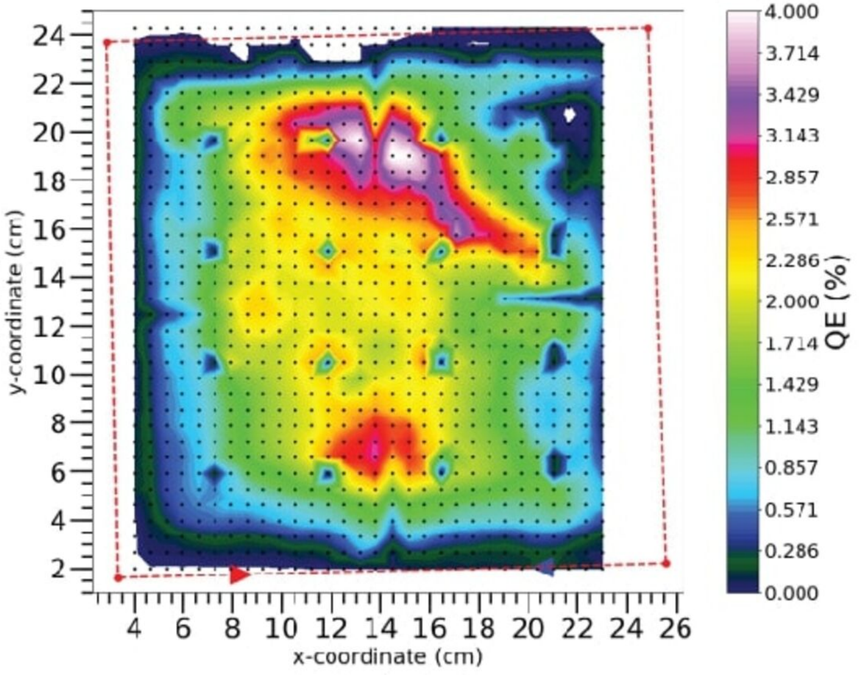

Micro-channel plate resistance over time during second round of cesium exposure

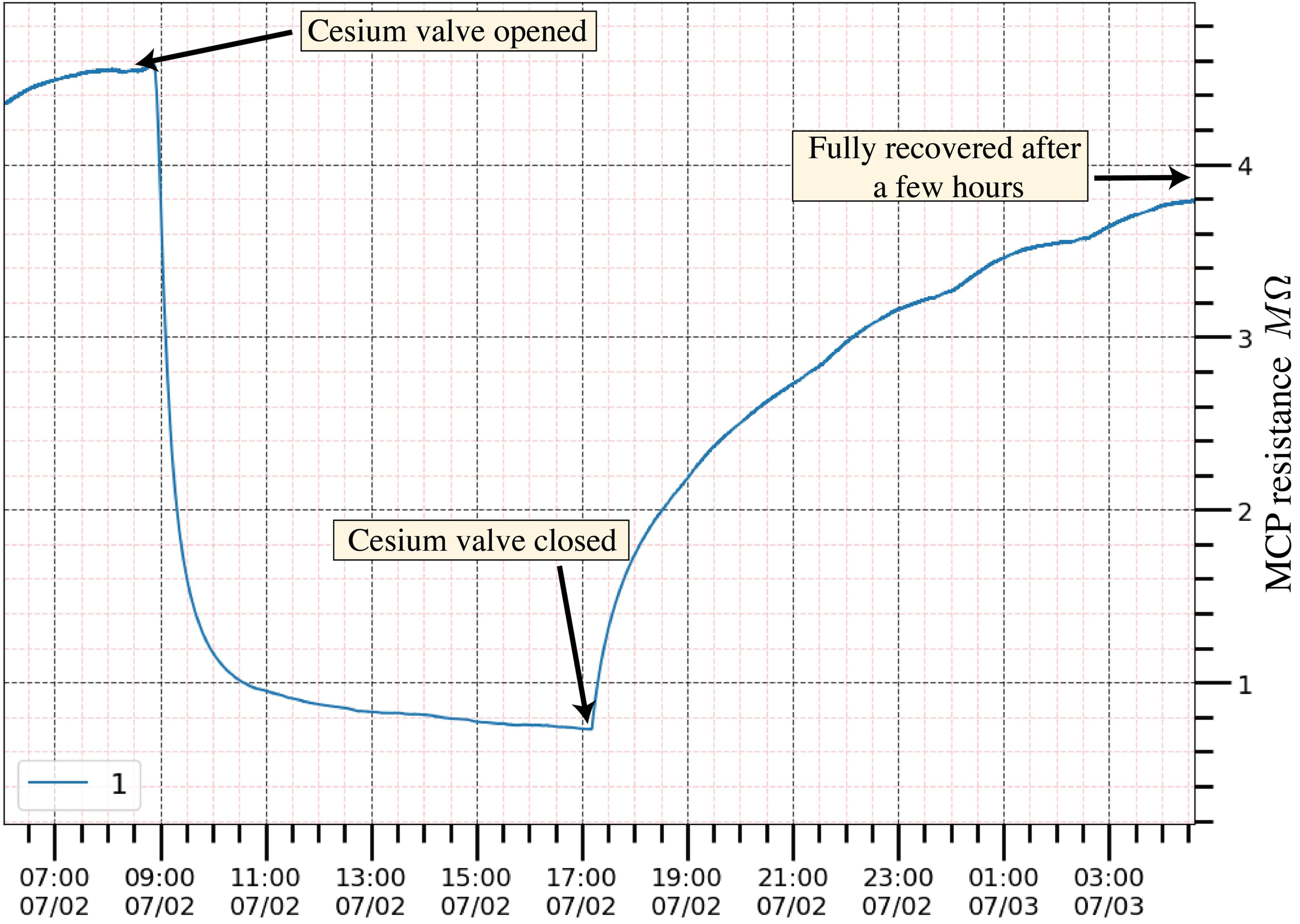

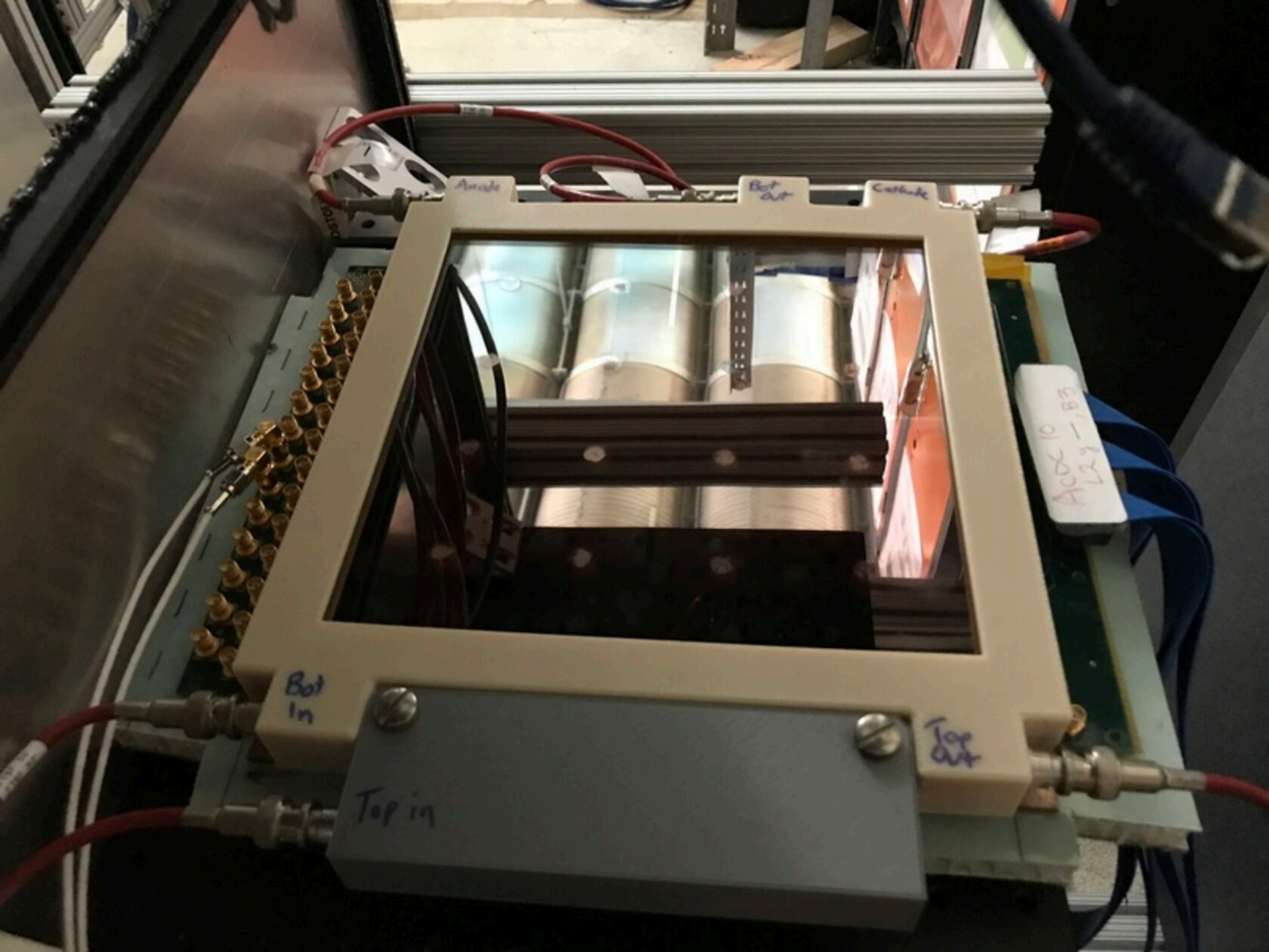
Anode
Bot Out
Cathode
Bot In
Top Out
Top in